Journal of
Composites Science

MDPI

Article

Strong and Weak Formulations of a Mixed Higher-Order Shear Deformation Theory for the Static Analysis of Functionally Graded Beams under Thermo-Mechanical Loads

Chih-Ping Wu * and Zhan-Rong Xu

Department of Civil Engineering, National Cheng Kung University, Tainan 70101, Taiwan; n66081147@gs.ncku.edu.tw
* Correspondence: cpwu@mail.ncku.edu.tw

Received: 1 October 2020; Accepted: 18 October 2020; Published: 23 October 2020

check for updates

Abstract: The strong and weak formulations of a mixed layer-wise (LW) higher-order shear deformation theory (HSDT) are developed for the static analysis of functionally graded (FG) beams under various boundary conditions subjected to thermo-mechanical loads. The material properties of the FG beam are assumed to obey a power-law distribution of the volume fractions of the constituents through the thickness of the FG beam, for which the effective material properties are estimated using the rule of mixtures, or it is directly assumed that the effective material properties of the FG beam obey an exponential function distribution along the thickness direction of the FG beam. The results shown in the numerical examples indicate that the mixed LW HSDT solutions for elastic and thermal field variables are in excellent agreement with the accurate solutions available in the literature. A parametric study related to various effects on the coupled thermo-mechanical behavior of FG beams is carried out, including the aspect ratio, the material-property gradient index, and different boundary conditions.

Keywords: coupled thermo-mechanical analyses; finite element methods; functionally graded beams; layer-wise beam theories; static; strong and weak formulations

1. Introduction

Functionally graded (FG) structures are emerging composite structures, for which material properties can be designed to gradually and smoothly vary through their physical domains. FG structures can be formed by mixing two-phase materials with pre-designed single- and bi-directional distributions of the volume fractions of the constituents through the thickness coordinate and the axial-thickness surface of the FG structures, respectively [1–5]. Due to their graded material properties, FG structures can prevent delamination and stress concentration phenomena, usually occurring at the interfaces between adjacent layers in the cases of laminated fiber-reinforced composite (FRC) structures as a result of the material properties suddenly changing at these locations. Some FG thermoelectric devices were developed to enhance their thermal stability resistance. For example, FG piezoelectric materials were developed for broad-band ultrasonic transducers [6] and FG composite electrodes were developed for solid oxide fuel cells [7]. The functional gradation principle was used to develop an artificial biomaterial for knee joint replacement [8]. Some FG materials were applied to optimize the thermal, wear, and corrosion properties of metallic and ceramic materials [9]. For example, FG thermal barrier coating materials were deposited onto Cu substrates to improve the interface fracture toughness between the coatings and the substrates. FG TiC-TiN thin films were used to improve the wear resistance of cutting tool alloys with good adhesion to the substrate material. FG materials were also developed as thermal barrier materials for space structures, fusion reactors, space plane systems, and turbine engines [10].

FG materials and structures are becoming increasingly more popular in various cutting-edge industries, including the aerospace, automobile, submarine, and nuclear industries. Assorted structural analyses of FG beams are thus attracting considerable attention [11,12]. Some equivalent single-layered theories (ESLTs) for laminated FRC beams have been reformulated to examine a variety of FG beam structural behaviors. Based on the Euler–Bernoulli theory (EBT), Sankar [13] examined the coupled thermo-mechanical behavior of simply supported, FG beams, where the thermo-elastic constants and the temperature changes were assumed to vary exponentially through the thickness direction of the beam. Using Hamilton's principle and Reddy's refined shear deformation theory (RSDT), Trinh et al. [14] developed a state space method for vibration and buckling analyses of FG beams under various boundary conditions when subjected to thermo-mechanical loads. Within the framework of the EBT, the first-order shear deformation theory (FSDT), and assorted higher-order shear deformation theories (HSDTs), Simsek [15] and Thai and Vo [16] investigated the bending and free vibration behavior of FG beams with different boundary conditions. Based on Carrera's unified formulation (CUF) [17], Giunta et al. [18] derived several ESLT-type beam theories to examine the coupled thermo-mechanical behavior of FG beams subjected to thermal loads. The above mentioned ESLTs, including EBT, FSDT, HSDT, and RSDT, can be regarded as special CUF cases, and they can be hierarchically derived using a fundamental nucleo. A comparative study for the stress and deformation behavior induced in laminated FRC beams was carried out by Carrera et al. [19] using a number of refined beam theories, for which the displacement components were expanded as Taylor's polynomials, trigonometric series, exponential, hyperbolic, and zig-zag functions through the thickness direction of the beam.

In order to capture the thickness effect on the structural behavior of laminated FRC beams and to accurately describe the zig-zag behavior of the through-thickness distributions of the in-plane displacement and in-plane stresses induced in laminated FRC beams, some layer-wise (LW) advanced and refined shear deformation theories, including the LW FSDTs, LW HSDTs, and LW RSDTs, have been proposed. Davalos et al. [20] and Mantari et al. [21] developed an LW constant shear theory and an LW trigonometric shear deformation theory (TSDT) for the analysis of laminated FRC beams, respectively. Wu and Kuo [22,23] presented a mixed LW HSDT for the static analysis of laminated FRC plates. Implementation of the mixed LW HSDT showed that its Navier's analytical solutions and finite element solutions were in excellent agreement with the exact 3D solutions available in the literature. Within the framework of the CUF, Yang et al. [24] and Filippi and Carrera [25] derived an LW refined, one-dimensional model and an LW zig-zag model for the bending and free vibration analyses of laminated FRC beams subjected to mechanical loads, respectively. Based on modified couple stress and FSDT, Yazdani Sarvestani et al. [26] conducted a size-dependent structural analysis of three-dimensional (3D) printable FG doubly curved panels. A comprehensive literature survey with regard to the articles examining the structural behavior of laminated structures using LW theories was carried out by Liew et al. [27].

Some exact and approximate 3D beam theories have also been developed to address the issue of interest in the present work. Vo et al. [28,29] and Nguyen et al. [30] developed a quasi-3D theory for the bending, free vibration, and buckling analyses of sandwiched FG beams, where both the shear deformation and thickness stretching effects were accounted for in the formulation by expanding the in-plane and out-of-plane displacement variables as a hyperbolic function distribution through the thickness direction of the beam. The mechanical behavior of two types of sandwiched FG beams were examined, where one type of sandwiched FG beam, composed of FG face sheets and a homogeneous core, and another type of sandwiched FG beam, composed of homogeneous face sheets and an FG core, were considered. Lü et al. [31] presented semi-analytical elasticity solutions for bi-directional FG beams subjected to thermo-mechanical loads using the state space differential quadrature (DQ) method, where variations in the thermal and elastic field variables with the thickness direction and the axial direction of the beam were analytically obtained using the state space method and numerically obtained using the DQ method, respectively. These quasi-3D solutions can provide a standard by which to assess the accuracy and convergence rates of assorted advanced and refined ESLTs and LW theories available in the literature.

After a close literature survey, it was found that most of the LW theories were applied to the mechanical analyses of laminated FRC beams and were rarely applied to the mechanical analyses of FG beams. Due to the excellent performance of the mixed LW HSDT [22,23], as mentioned above, the authors extend it to the current coupled thermo-mechanical analysis of FG beams with various boundary conditions. In the formulation, the displacement components are expanded as an LW third-order polynomial function through the thickness direction of the beam, and the displacement continuity conditions at the interfaces between adjacent layers are introduced in the potential energy functional using the Lagrange multiplier method, such that they are satisfied in a variational form. The Lagrange multipliers are the exact transverse stress components. Based on the stationary principle of the extended potential functional, the strong and weak formulations of the mixed LW HSDT are derived. The Navier-type analytical solutions based on the strong formulation and the finite element (FE) solutions based on the weak formulation for the static analysis of FG beams subjected to thermo-mechanical loads are obtained. The accuracy and convergence rates of these analytical and finite element solutions are validated by comparing them with the quasi-3D solutions available in the literature. Some effects on the coupled thermo-mechanical behavior of FG beams are conducted, including the aspect ratio, the material-property gradient index, and different boundary conditions.

2. Effective Material Properties

In this work, the rule of mixtures [32] is used to estimate the effective material properties of the FG beam and is described as follows:

According to the rule of mixtures, the through-thickness distributions of the effective material properties of the FG beam can be written in the following form,

$$\begin{aligned} F_{eff}(z) &= \Gamma_c(z)F_c + \Gamma_m(z)F_m \\ &= F_m + (F_c - F_m)\Gamma_c(z) \end{aligned} \tag{1}$$

where Γ_c and Γ_m represent the volume fractions of the ceramic and metal materials of the constituents of the FG beam, respectively, such that $\Gamma_m + \Gamma_c = 1$. F can be one of the engineering constants, including Young's modulus E, Poisson's ratio υ, thermal expansion coefficient α, and mass density ρ. The subscripts m and c represent a metal material and a ceramic material, respectively.

3. The Strong Formulation and Its Application

In this section, the authors develop the strong formulation of a mixed LW HSDT for a static analysis of FG beams under various boundary conditions subjected to thermo-mechanical loads, where the material properties of the FG beam are considered to be thickness dependent. The configuration and coordinates of the FG beam are shown in Figure 1, where h and L represent the thickness and the length of the FG beam, respectively. In the analysis, the FG beam is artificially divided into n_l layers, and the thickness of each individual layer constituting the beam is h_m ($m = 1 - n_l$), such that $\sum_{m=1}^{n_l} h_m = h$.

In the mixed LW HSDT, the displacement field for a typical individual layer is given as follows:

$$u^{(m)}(x, z_m) = u_0^{(m)}(x) + z_m\, u_1^{(m)}(x) + z_m^2\, u_2^{(m)}(x) + z_m^3\, u_3^{(m)}(x), \tag{2}$$

$$w^{(m)}(x, z_m) = w_0^{(m)}(x) + z_m\, w_1^{(m)}(x) + z_m^2\, w_2^{(m)}(x) + z_m^3\, w_3^{(m)}(x), \tag{3}$$

where $m = 1, 2, \ldots, n_l$, and $u_0^{(m)}$ and $w_0^{(m)}$ denote the mid-plane displacements of the layer in the x and z directions, respectively, and their ith-order expansion terms along the local thickness direction are $u_i^{(m)}$ and $w_i^{(m)}$ $(i = 1,\ 2,\ \text{and}\ 3)$. The displacement components in the y direction are taken to be zero.

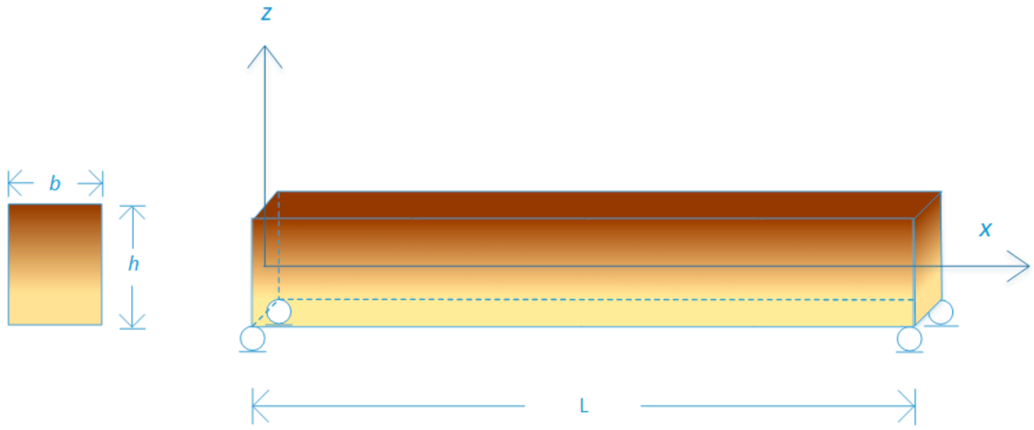

Figure 1. Configurations and coordinate systems of a functionally graded (FG) beam.

According to the perfect bonding assumptions at the interfaces between adjacent layers, the corresponding displacement continuity conditions at these locations are given as

$$\begin{aligned} f_x^{(k)} &= \left[u_0^{(k+1)} - (h_{k+1}/2)\,u_1^{(k+1)} + \left(h_{k+1}^2/4\right)u_2^{(k+1)} - \left(h_{k+1}^3/8\right)u_3^{(k+1)}\right] \\ &\quad -\left[u_0^{(k)} + (h_k/2)\,u_1^{(k)} + \left(h_k^2/4\right)u_2^{(k)} + \left(h_k^3/8\right)u_3^{(k)}\right] \\ &= 0, \end{aligned} \tag{4}$$

$$\begin{aligned} f_z^{(k)} &= \left[w_0^{(k+1)} - (h_{k+1}/2)\,w_1^{(k+1)} + \left(h_{k+1}^2/4\right)w_2^{(k+1)} - \left(h_{k+1}^3/8\right)w_3^{(k+1)}\right] \\ &\quad -\left[w_0^{(k)} + (h_k/2)\,w_1^{(k)} + \left(h_k^2/4\right)w_2^{(k)} + \left(h_k^3/8\right)w_3^{(k)}\right] \\ &= 0, \end{aligned} \tag{5}$$

where $k = 1, 2, \ldots, (n_l - 1)$.

The strain–displacement relationship is given as

$$\begin{aligned} \varepsilon_x^{(m)} &= \left(\varepsilon_x^{(m)}\right)_l + \left(\varepsilon_x^{(m)}\right)_{nl} \\ &= \left(u_0^{(m)}{}_{,x} + z_m\, u_1^{(m)}{}_{,x} + z_m^2\, u_2^{(m)}{}_{,x} + z_m^3\, u_3^{(m)}{}_{,x}\right), \end{aligned} \tag{6}$$

$$\begin{aligned} \varepsilon_z^{(m)} &= w^{(m)}{}_{,z_m} \\ &= w_1^{(m)} + 2\,z_m\, w_2^{(m)} + 3z_m^2\, w_3^{(m)}, \end{aligned} \tag{7}$$

$$\begin{aligned} \gamma_{xz}^{(m)} &= u^{(m)}{}_{,z_m} + w^{(m)}{}_{,x} \\ &= \left(w_0^{(m)}{}_{,x} + u_1^{(m)}\right) + z_m\left(w_1^{(m)}{}_{,x} + 2\,u_2^{(m)}\right) + z_m^2\left(w_2^{(m)}{}_{,x} + 3\,u_3^{(m)}\right) + z_m^3\left(w_3^{(m)}{}_{,x}\right), \end{aligned} \tag{8}$$

where the commas denote the derivative of the suffix variable, and the remaining strains are zeroes, including $\varepsilon_y^{(m)}$, $\gamma_{yz}^{(m)}$, and $\gamma_{xy}^{(m)}$.

The stress–strain relationship for an orthotropic material in thermal environment is given as

$$\begin{Bmatrix} \sigma_x^{(m)} \\ \sigma_z^{(m)} \\ \tau_{xz}^{(m)} \end{Bmatrix} = \begin{bmatrix} Q_{11}^{(m)} & Q_{13}^{(m)} & 0 \\ Q_{13}^{(m)} & Q_{33}^{(m)} & 0 \\ 0 & 0 & Q_{55}^{(m)} \end{bmatrix} \left(\begin{Bmatrix} \varepsilon_x^{(m)} \\ \varepsilon_z^{(m)} \\ \gamma_{xz}^{(m)} \end{Bmatrix} - \begin{Bmatrix} Q_{1\alpha}^{(m)} \\ Q_{3\alpha}^{(m)} \\ 0 \end{Bmatrix} \Delta T, \right) \tag{9}$$

where ΔT denotes the temperature change, measured at a room temperature of 300 K. $Q_{11}^{(m)} = [(1 - \upsilon_{23}\upsilon_{32})/(E_2\,E_3\,\Delta)]^{(m)}$, $Q_{13}^{(m)} = [(\upsilon_{13} + \upsilon_{12}\upsilon_{32})/(E_1\,E_2\,\Delta)]^{(m)}$, $Q_{33}^{(m)} = [(1 - \upsilon_{12}\upsilon_{21})/(E_1\,E_2\,\Delta)]^{(m)}$,

$Q_{55}^{(m)} = G_{13}$, $\Delta = [(1 - \upsilon_{12}\upsilon_{21} - \upsilon_{23}\upsilon_{32} - \upsilon_{31}\upsilon_{13} - 2\upsilon_{21}\upsilon_{32}\upsilon_{13})/(E_1 E_2 E_3)]^{(m)}$, $Q_{1\alpha}^{(m)} = Q_{11}^{(m)} \alpha_1^{(m)} + Q_{13}^{(m)} \alpha_3^{(m)}$, $Q_{3\alpha}^{(m)} = Q_{13}^{(m)} \alpha_1^{(m)} + Q_{33}^{(m)} \alpha_3^{(m)}$ in which the subscripts 1, 2, and 3 denote the principle axes of the material properties, and E, α and υ and represent the Young's modulus, the thermal expansion coefficients, and Poisson's ratio, respectively. For isotropic materials, these stiffness coefficients will be reduced to $Q_{11}^{(m)} = Q_{33}^{(m)} = \{E\,\upsilon/[(1+\upsilon)\,(1-2\upsilon)]\}^{(m)}$, $Q_{13}^{(m)} = \{E\,\upsilon/[(1+\upsilon)\,(1-2\upsilon)]\}^{(m)}$, $Q_{55}^{(m)} = \{E\,/[2(1+\upsilon)]\}^{(m)}$, and $\alpha_1^{(m)} = \alpha_3^{(m)} = \alpha$. Note that these engineering constants E, α and υ in the analysis are considered to be dependent from the thickness of the FG beam, where ΔT is a function of x and z, i.e., $\Delta T(x,\ z)$.

The governing equations and associated boundary conditions are derived using the stationary principle of minimum potential energy combined with the Lagrange multiplier method, in which the displacement continuity conditions at the interfaces between adjacent layers given in Equations (4) and (5) are multiplied by the Lagrange multipliers and are then substituted into the potential energy functional as the constraints, such that the extended potential energy functional of the n_l-layered FG beam can be given as follows:

$$\begin{aligned}\Pi_p = &\sum_{m=1}^{n_l} \int_0^L \int_{-h_m/2}^{h_m/2} \Big[(1/2)\,\sigma_x^{(m)}\,\varepsilon_x^{(m)} + (1/2)\,\sigma_z^{(m)}\,\varepsilon_z^{(m)} + (1/2)\,\tau_{xz}^{(m)}\,\gamma_{xz}^{(m)}\Big] dz_m\,dx + \int_0^L q(x)\,w^{(n_l)}\left(x,\, z_{n_l} = h_{n_l}/2\right) dx \\ &- \left[\sum_{m=1}^{n_l} \int_{-h_m/2}^{h_m/2} \left(\overline{\sigma}_x^{(m)} u^{(m)} + \overline{\tau}_{xz}^{(m)} w^{(m)}\right) dz_m\right]\Bigg|_{x=0}^{x=L} + \sum_{k=1}^{(n_l-1)} \int_0^L \left[\left(\lambda_x^{(k)}\right)\left(f_x^{(k)}\right) + \left(\lambda_z^{(k)}\right)\left(f_z^{(k)}\right)\right] dx,\end{aligned} \tag{10}$$

where $\overline{\sigma}_x^{(m)}$ and $\overline{\tau}_{xz}^{(m)}$ are the traction stresses applied on the edges, and $\lambda_x^{(m)}$ and $\lambda_z^{(m)}$ are the Lagrange multipliers, which are identical to the transverse shear and normal stress components (i.e., $\tau_{xz}^{(m)}$ and $\sigma_z^{(m)}$) induced at the interfaces between adjacent layers, respectively. $q(x)$ is the external load applied on the top surface of the FG beam, where its positive direction is defined to be downward.

Applying the stationary principle of minimum potential energy, following a standard variational process, and integrating the stress variables through the thickness direction of the beam, the authors obtain

$$\begin{aligned}\delta\,\Pi_p = &\sum_{m=1}^{n_l} \int_0^L \Big\{\left(N_x^{(m)} - N_{xt}^{(m)}\right)\delta\,u_{0}^{(m)}{}_{,x} + \left(M_x^{(m)} - M_{xt}^{(m)}\right)\delta u_{1}^{(m)}{}_{,x} + \left(P_x^{(m)} - P_{xt}^{(m)}\right)\delta u_{2}^{(m)}{}_{,x} + \left(R_x^{(m)} - R_{xt}^{(m)}\right)\delta u_{3}^{(m)}{}_{,x} \\ &+ \left(N_z^{(m)} - N_{zt}^{(m)}\right)\delta\,w_1^{(m)} + 2\left(M_z^{(m)} - M_{zt}^{(m)}\right)\delta w_2^{(m)} + 3\left(P_z^{(m)} - P_{zt}^{(m)}\right)\delta w_3^{(m)} \\ &+ N_{xz}^{(m)}\left(\delta\,w_{0}^{(m)}{}_{,x} + \delta\,u_1^{(m)}\right) + M_{xz}^{(m)}\left(\delta\,w_{1}^{(m)}{}_{,x} + 2\delta\,u_2^{(m)}\right) + P_{xz}^{(m)}\left(\delta\,w_{2}^{(m)}{}_{,x} + 3\delta\,u_3^{(m)}\right) + R_{xz}^{(m)}\left(\delta\,w_{3}^{(m)}{}_{,x}\right)\Big\}\,dx \\ &+ \int_0^L q(x)\left[\delta w_0^{(n_l)} + \left(h_{n_l}/2\right)\delta w_1^{(n_l)} + \left(h_{n_l}^2/4\right)\delta w_2^{(n_l)} + \left(h_{n_l}^3/8\right)\delta w_3^{(n_l)}\right] dx \\ &+ \sum_{k=1}^{(n_l-1)} \int_0^L \left[\left(\delta\lambda_x^{(k)}\right)\left(f_x^{(k)}\right) + \left(\delta\lambda_z^{(k)}\right)\left(f_z^{(k)}\right) + \left(\lambda_x^{(k)}\right)\left(\delta f_x^{(k)}\right) + \left(\lambda_z^{(k)}\right)\left(\delta f_z^{(k)}\right)\right] dx + (\text{boundary terms}) \\ &= 0,\end{aligned} \tag{11}$$

where $\begin{bmatrix} N_x^{(m)} & N_z^{(m)} & N_{xz}^{(m)} \\ M_x^{(m)} & M_z^{(m)} & M_{xz}^{(m)} \\ P_x^{(m)} & P_z^{(m)} & P_{xz}^{(m)} \end{bmatrix} = \int_{-h_m/2}^{h_m/2} \begin{Bmatrix} 1 \\ z_m \\ z_m^2 \end{Bmatrix} \begin{Bmatrix} \sigma_x^{(m)} & \sigma_z^{(m)} & \tau_{xz}^{(m)} \end{Bmatrix} dz_m,$, $\begin{Bmatrix} R_x^{(m)} & R_{xz}^{(m)} \end{Bmatrix} = \int_{-h_m/2}^{h_m/2} z_m^3 \begin{Bmatrix} \sigma_x^{(m)} & \tau_{xz}^{(m)} \end{Bmatrix} dz_m$,

$$\begin{bmatrix} N_{xt}^{(m)} & N_{zt}^{(m)} \\ M_{xt}^{(m)} & M_{zt}^{(m)} \\ P_{xt}^{(m)} & P_{zt}^{(m)} \end{bmatrix} = \int_{-h_m/2}^{h_m/2} \begin{Bmatrix} 1 \\ z_m \\ z_m^2 \end{Bmatrix} \begin{Bmatrix} Q_{1\alpha}^{(m)}\Delta T & Q_{3\alpha}^{(m)}\Delta T \end{Bmatrix} dz_m,\ R_{xt}^{(m)} = \int_{-h_m/2}^{h_m/2} z_m^3\, Q_{1\alpha}^{(m)}\,\Delta T\,dz_m.$$

Performing Equation (11), the integration by part yields

$$
\begin{aligned}
\delta\Pi_p = & \sum_{m=1}^{n_l}\int_0^L\Big\{-\left(N_x^{(m)}-N_{xt}^{(m)}\right)_{,x}\delta u_0^{(m)}-\left(M_x^{(m)}-M_{xt}^{(m)}\right)_{,x}\delta u_1^{(m)}-\left(P_x^{(m)}-P_{xt}^{(m)}\right)_{,x}\delta u_2^{(m)}-\left(R_x^{(m)}-R_{xt}^{(m)}\right)_{,x}\delta u_3^{(m)}\\
& +\left(N_z^{(m)}-N_{zt}^{(m)}\right)\delta w_1^{(m)}+2\left(M_z^{(m)}-M_{zt}^{(m)}\right)\delta w_2^{(m)}+3\left(P_z^{(m)}-P_{zt}^{(m)}\right)\delta w_3^{(m)}\\
& -N_{xz}^{(m)}{}_{,x}\,\delta w_0^{(m)}+N_{xz}^{(m)}\delta u_1^{(m)}-M_{xz}^{(m)}{}_{,x}\,\delta w_1^{(m)}+2M_{xz}^{(m)}\delta u_2^{(m)}-P_{xz}^{(m)}{}_{,x}\,\delta w_2^{(m)}+3P_{xz}^{(m)}\delta u_3^{(m)}-R_{xz}^{(m)}{}_{,x}\,\delta w_3^{(m)}\Big\}dx\\
& +\int_0^L q(x)\left[\delta w_0^{(n_l)}+\left(h_{n_l}/2\right)\delta w_1^{(n_l)}+\left(h_{n_l}^2/4\right)\delta w_2^{(n_l)}+\left(h_{n_l}^3/8\right)\delta w_3^{(n_l)}\right]dx\\
& +\sum_{k=1}^{(n_l-1)}\int_0^L\left[\left(\delta\lambda_x^{(k)}\right)\left(f_x^{(k)}\right)+\left(\delta\lambda_z^{(k)}\right)\left(f_z^{(k)}\right)+\left(\lambda_x^{(k)}\right)\left(\delta f_x^{(k)}\right)+\left(\lambda_z^{(k)}\right)\left(\delta f_z^{(k)}\right)\right]dx+(\text{boundary terms})\\
& =0,
\end{aligned}
\tag{12}
$$

According to Equation (12), the Euler–Lagrange equations of the mixed LW HSDT can be obtained as follows:

$$\delta u_0^{(m)}:\ -N_x^{(m)}{}_{,x}+\left(\lambda_x^{(m-1)}-\lambda_x^{(m)}\right)=-N_{xt}^{(m)}{}_{,x}\,, \tag{13}$$

$$\delta u_1^{(m)}:\ -M_x^{(m)}{}_{,x}+N_{xz}^{(m)}+(-h_m/2)\left(\lambda_x^{(m-1)}+\lambda_x^{(m)}\right)=-M_{xt}^{(m)}{}_{,x}\,, \tag{14}$$

$$\delta u_2^{(m)}:\ -P_x^{(m)}{}_{,x}+2M_{xz}^{(m)}+\left(h_m^2/4\right)\left(\lambda_x^{(m-1)}-\lambda_x^{(m)}\right)=-P_{xt}^{(m)}{}_{,x}\,, \tag{15}$$

$$\delta u_3^{(m)}:\ -R_x^{(m)}{}_{,x}+3P_{xz}^{(m)}+\left(-h_m^3/8\right)\left(\lambda_x^{(m-1)}+\lambda_x^{(m)}\right)=-R_{xt}^{(m)}{}_{,x}\,, \tag{16}$$

$$\delta w_0^{(m)}:\ -N_{xz}^{(m)}{}_{,x}+\left(\lambda_z^{(m-1)}-\lambda_z^{(m)}\right)=-\delta_{mn_l}\,q(x), \tag{17}$$

$$\delta w_1^{(m)}:\ -M_{xz}^{(m)}{}_{,x}+N_z^{(m)}+(-h_m/2)\left(\lambda_z^{(m-1)}+\lambda_z^{(m)}\right)=-\delta_{mn_l}\left(h_{n_l}/2\right)q(x)+N_{zt}^{(m)}, \tag{18}$$

$$\delta w_2^{(m)}:\ -P_{xz}^{(m)}{}_{,x}+2M_z^{(m)}+\left(h_m^2/4\right)\left(\lambda_z^{(m-1)}-\lambda_z^{(m)}\right)=-\delta_{mn_l}\left(h_{n_l}^2/4\right)q(x)+2M_{zt}^{(m)}, \tag{19}$$

$$\delta w_3^{(m)}:\ -R_{xz}^{(m)}{}_{,x}+3P_z^{(m)}+\left(-h_m^3/8\right)\left(\lambda_z^{(m-1)}+\lambda_z^{(m)}\right)=-\delta_{mn_l}\left(h_{n_l}^3/8\right)q(x)+3P_{zt}^{(m)}, \tag{20}$$

$$\delta\lambda_x^{(k)}:\ f_x^{(k)}=0, \tag{21}$$

$$\delta\lambda_z^{(k)}:\ f_z^{(k)}=0, \tag{22}$$

where $m = 1, 2, \ldots, n_l$ and $k = 1, 2, \ldots, (n_l - 1)$.

The possible boundary conditions are given as

$$\text{Either } N_x^{(m)}=\overline{N}_x^{(m)}+N_{xt}^{(m)} \text{ or } u_0^{(m)}=\overline{u}_0^{(m)}, \tag{23}$$

$$\text{Either } M_x^{(m)}=\overline{M}_x^{(m)}+M_{xt}^{(m)} \text{ or } u_1^{(m)}=\overline{u}_1^{(m)}, \tag{24}$$

$$\text{Either } P_x^{(m)}=\overline{P}_x^{(m)}+P_{xt}^{(m)} \text{ or } u_2^{(m)}=\overline{u}_2^{(m)}, \tag{25}$$

$$\text{Either } R_x^{(m)}=\overline{R}_x^{(m)}+R_{xt}^{(m)} \text{ or } u_3^{(m)}=\overline{u}_3^{(m)}, \tag{26}$$

$$\text{Either } N_{xz}^{(m)}=\overline{N}_{xz}^{(m)} \text{ or } w_0^{(m)}=\overline{w}_0^{(m)}, \tag{27}$$

$$\text{Either } M_{xz}^{(m)}=\overline{M}_{xz}^{(m)} \text{ or } w_1^{(m)}=\overline{w}_1^{(m)}, \tag{28}$$

$$\text{Either } P_{xz}^{(m)}=\overline{P}_{xz}^{(m)} \text{ or } w_2^{(m)}=\overline{w}_2^{(m)}, \text{ and} \tag{29}$$

$$\text{Either } R_{xz}^{(m)}=\overline{R}_{xz}^{(m)} \text{ or } w_3^{(m)}=\overline{w}_3^{(m)}, \tag{30}$$

where $\overline{u}_i^{(m)}$ and $\overline{w}_i^{(m)}$ ($i = 0$, 1, 2, and 3) are the prescribed displacement components on the edges.

The definition of each force resultant component and its relationship with the displacement components are given in Appendix A.

Substituting Equations (A1)–(A11) into Equations (13)–(22), the authors obtain the Euler–Lagrange equations of the mixed LW HSDT in terms of all displacement components, which are given as follows:

$$\begin{aligned}\delta u_0^{(m)} :\ & -A_{11}^{(m)} u_0^{(m)}{}_{,xx} - B_{11}^{(m)} u_1^{(m)}{}_{,xx} - D_{11}^{(m)} u_2^{(m)}{}_{,xx} - F_{11}^{(m)} u_3^{(m)}{}_{,xx} \\ & -A_{13}^{(m)} w_1^{(m)}{}_{,x} - 2B_{13}^{(m)} w_2^{(m)}{}_{,x} - 3D_{13}^{(m)} w_3^{(m)}{}_{,x} + \left(\lambda_x^{(m-1)} - \lambda_x^{(m)}\right) = -N_{xt}^{(m)}{}_{,x},\end{aligned} \tag{31}$$

$$\begin{aligned}\delta u_1^{(m)} :\ & -B_{11}^{(m)} u_0^{(m)}{}_{,xx} - D_{11}^{(m)} u_1^{(m)}{}_{,xx} - F_{11}^{(m)} u_2^{(m)}{}_{,xx} - H_{11}^{(m)} u_3^{(m)}{}_{,xx} - B_{13}^{(m)} w_1^{(m)}{}_{,x} \\ & -2D_{13}^{(m)} w_2^{(m)}{}_{,x} - 3F_{13}^{(m)} w_3^{(m)}{}_{,x} + A_{55}^{(m)}\left(w_0^{(m)}{}_{,x} + u_1^{(m)}\right) + B_{55}^{(m)}\left(w_1^{(m)}{}_{,x} + 2u_2^{(m)}\right) \\ & + D_{55}^{(m)}\left(w_2^{(m)}{}_{,x} + 3u_3^{(m)}\right) + F_{55}^{(m)} w_3^{(m)}{}_{,x} + (-h_m/2)\left(\lambda_x^{(m-1)} + \lambda_x^{(m)}\right) = -M_{xt}^{(m)}{}_{,x},\end{aligned} \tag{32}$$

$$\begin{aligned}\delta u_2^{(m)} :\ & -D_{11}^{(m)} u_0^{(m)}{}_{,xx} - F_{11}^{(m)} u_1^{(m)}{}_{,xx} - H_{11}^{(m)} u_2^{(m)}{}_{,xx} - J_{11}^{(m)} u_3^{(m)}{}_{,xx} - D_{13}^{(m)} w_1^{(m)}{}_{,x} \\ & -2F_{13}^{(m)} w_2^{(m)}{}_{,x} - 3H_{13}^{(m)} w_3^{(m)}{}_{,x} + 2B_{55}^{(m)}\left(w_0^{(m)}{}_{,x} + u_1^{(m)}\right) + 2D_{55}^{(m)}\left(w_1^{(m)}{}_{,x} + 2u_2^{(m)}\right) \\ & + 2F_{55}^{(m)}\left(w_2^{(m)}{}_{,x} + 3u_3^{(m)}\right) + 2H_{55}^{(m)} w_3^{(m)}{}_{,x} + \left(h_m^2/4\right)\left(\lambda_x^{(m-1)} - \lambda_x^{(m)}\right) = -P_{xt}^{(m)}{}_{,x},\end{aligned} \tag{33}$$

$$\begin{aligned}\delta u_3^{(m)} :\ & -F_{11}^{(m)} u_0^{(m)}{}_{,xx} - H_{11}^{(m)} u_1^{(m)}{}_{,xx} - J_{11}^{(m)} u_2^{(m)}{}_{,xx} - L_{11}^{(m)} u_3^{(m)}{}_{,xx} - F_{13}^{(m)} w_1^{(m)}{}_{,x} \\ & -2H_{13}^{(m)} w_2^{(m)}{}_{,x} - 3J_{13}^{(m)} w_3^{(m)}{}_{,x} + 3D_{55}^{(m)}\left(w_0^{(m)}{}_{,x} + u_1^{(m)}\right) + 3F_{55}^{(m)}\left(w_1^{(m)}{}_{,x} + 2u_2^{(m)}\right) \\ & + 3H_{55}^{(m)}\left(w_2^{(m)}{}_{,x} + 3u_3^{(m)}\right) + 3J_{55}^{(m)} w_3^{(m)}{}_{,x} + \left(-h_m^3/8\right)\left(\lambda_x^{(m-1)} + \lambda_x^{(m)}\right) = -R_{xt}^{(m)}{}_{,x},\end{aligned} \tag{34}$$

$$\begin{aligned}\delta w_0^{(m)} :\ & -A_{55}^{(m)}\left(w_0^{(m)}{}_{,xx} + u_1^{(m)}{}_{,x}\right) - B_{55}^{(m)}\left(w_1^{(m)}{}_{,xx} + 2u_2^{(m)}{}_{,x}\right) - D_{55}^{(m)}\left(w_2^{(m)}{}_{,xx} + 3u_3^{(m)}{}_{,x}\right) \\ & -F_{55}^{(m)} w_3^{(m)}{}_{,xx} + \left(\lambda_z^{(m-1)} - \lambda_z^{(m)}\right) = -\delta_{mn_l}\, q(x),\end{aligned} \tag{35}$$

$$\begin{aligned}\delta w_1^{(m)} :\ & -B_{55}^{(m)}\left(w_0^{(m)}{}_{,xx} + u_1^{(m)}{}_{,x}\right) - D_{55}^{(m)}\left(w_1^{(m)}{}_{,xx} + 2u_2^{(m)}{}_{,x}\right) - F_{55}^{(m)}\left(w_2^{(m)}{}_{,xx} + 3u_3^{(m)}{}_{,x}\right) \\ & -H_{55}^{(m)} w_3^{(m)}{}_{,xx} + A_{13}^{(m)} u_0^{(m)}{}_{,x} + B_{13}^{(m)} u_1^{(m)}{}_{,x} + D_{13}^{(m)} u_2^{(m)}{}_{,x} + F_{13}^{(m)} u_3^{(m)}{}_{,x} + A_{33}^{(m)} w_1^{(m)} \\ & + 2B_{33}^{(m)} w_2^{(m)} + 3D_{33}^{(m)} w_3^{(m)} + (-h_m/2)\left(\lambda_z^{(m-1)} + \lambda_z^{(m)}\right) = -\delta_{mn_l}\left(h_{n_l}/2\right) q(x) + N_{zt}^{(m)},\end{aligned} \tag{36}$$

$$\begin{aligned}\delta w_2^{(m)} :\ & -D_{55}^{(m)}\left(w_0^{(m)}{}_{,xx} + u_1^{(m)}{}_{,x}\right) - F_{55}^{(m)}\left(w_1^{(m)}{}_{,xx} + 2u_2^{(m)}{}_{,x}\right) - H_{55}^{(m)}\left(w_2^{(m)}{}_{,xx} + 3u_3^{(m)}{}_{,x}\right) \\ & -J_{55}^{(m)} w_3^{(m)}{}_{,xx} + 2B_{13}^{(m)} u_0^{(m)}{}_{,x} + 2D_{13}^{(m)} u_1^{(m)}{}_{,x} + 2F_{13}^{(m)} u_2^{(m)}{}_{,x} + 2H_{13}^{(m)} u_3^{(m)}{}_{,x} + 2B_{33}^{(m)} w_1^{(m)} \\ & + 4D_{33}^{(m)} w_2^{(m)} + 6F_{33}^{(m)} w_3^{(m)} + \left(h_m^2/4\right)\left(\lambda_z^{(m-1)} - \lambda_z^{(m)}\right) = -\delta_{mn_l}\left(h_m^2/4\right) q(x) + 2M_{zt}^{(m)},\end{aligned} \tag{37}$$

$$\begin{aligned}\delta w_3^{(m)} :\ & -F_{55}^{(m)}\left(w_0^{(m)}{}_{,xx} + u_1^{(m)}{}_{,x}\right) - H_{55}^{(m)}\left(w_1^{(m)}{}_{,xx} + 2u_2^{(m)}{}_{,x}\right) - J_{55}^{(m)}\left(w_2^{(m)}{}_{,xx} + 3u_3^{(m)}{}_{,x}\right) \\ & -L_{55}^{(m)} w_3^{(m)}{}_{,xx} + 3D_{13}^{(m)} u_0^{(m)}{}_{,x} + 3F_{13}^{(m)} u_1^{(m)}{}_{,x} + 3H_{13}^{(m)} u_2^{(m)}{}_{,x} + 3J_{13}^{(m)} u_3^{(m)}{}_{,x} + 3D_{33}^{(m)} w_1^{(m)} \\ & + 6F_{33}^{(m)} w_2^{(m)} + 9H_{33}^{(m)} w_3^{(m)} + \left(-h_m^3/8\right)\left(\lambda_z^{(m-1)} + \lambda_z^{(m)}\right) = -\delta_{mn_l}\left(-h_m^3/8\right) q(x) + 3P_{zt}^{(m)},\end{aligned} \tag{38}$$

$$\delta\lambda_x^{(k)} :\ f_x^{(k)} = 0, \tag{39}$$

$$\delta\lambda_z^{(k)} :\ f_z^{(k)} = 0, \tag{40}$$

where $m = 1, 2, \ldots, n_l$ and $k = 1, 2, \ldots, (n_l - 1)$.

The total number of Euler–Lagrange equations, i.e., Equations (31)–(40), is $(10n_l - 2)$, $(8n_l - 2)$, and $(6n_l - 2)$ for the mixed layer-wise third-order (LW3), second-order (LW2), and first-order (LW1) shear deformation theories, respectively, which are taken in terms of the same number of unknowns as those in the corresponding Euler–Lagrange equations. The strong formulation of the mixed LW

HSDT is thus obtained, including the Euler–Lagrange equations (Equations (31)–(40)) and the possible boundary conditions (Equations (23)–(30)).

Equations (31)–(40), associated with a set of boundary conditions (i.e., Equations (23)–(30)), can be composed of a well-post boundary value problem, for which the Navier-type analytical solutions of the elastic and thermal variables induced in simply supported, multi-layered FG beams can be obtained using the Fourier series expansion method, for which the detailed solution process is given in Appendix B.

4. The Weak Formulation and Its Application

To develop the weak formulation of the mixed LW HSDT, the authors perform the first-order variational operation with respect to the potential energy functional of the multi-layered FG beams, as follows:

$$\begin{aligned}\delta\Pi_p = &\sum_{m=1}^{n_l}\sum_{e=1}^{n_e}\int_{x_e}^{x_{e+1}}\int_{-h_m/2}^{h_m/2}\left[\sigma_x^{(m)}\,\delta\varepsilon_x^{(m)} + \sigma_z^{(m)}\,\delta\varepsilon_z^{(m)} + \tau_{xz}^{(m)}\,\delta\gamma_{xz}^{(m)}\right]dz_m\,dx + \int_0^L q(x)\left[\delta w\left(x,\,z_{n_l} = h_{n_l}/2\right)\right]^{(n_l)}dx \\ &-\left[\sum_{m=1}^{n_l}\int_{-h_m/2}^{h_m/2}\left(\overline{\sigma}_x^{(m)}\,\delta u^{(m)} + \overline{\tau}_{xz}^{(m)}\,\delta w^{(m)}\right)dz_m\right]\Bigg|_{x=0}^{x=L} \\ &+\sum_{k=1}^{(n_l-1)}\int_{x_e}^{x_{e+1}}\left[\left(\delta\lambda_x^{(k)}\right)\left(f_x^{(k)}\right) + \left(\delta\lambda_z^{(k)}\right)\left(f_z^{(k)}\right) + \left(\lambda_x^{(k)}\right)\left(\delta f_x^{(k)}\right) + \left(\lambda_z^{(k)}\right)\left(\delta f_z^{(k)}\right)\right]dx \\ &= 0,\end{aligned} \tag{41}$$

where n_e denotes the number of nodes used for a typical element.

The primary variables are expressed as

$$\left\{\begin{array}{cccc}\left(u_l^{(e)}\right)^{(m)} & \left(w_l^{(e)}\right)^{(m)} & \left(\lambda_x^{(e)}\right)^{(k)} & \left(\lambda_z^{(e)}\right)^{(k)}\end{array}\right\} = \sum_{i=1}^{n_d}\left\{\begin{array}{cccc}\left(u_l^{(e)}\right)_i^{(m)} & \left(w_l^{(e)}\right)_i^{(m)} & \left(\lambda_x^{(e)}\right)_i^{(k)} & \left(\lambda_z^{(e)}\right)_i^{(k)}\end{array}\right\}\psi_i^{(e)}\ (l = 0\text{–}3), \tag{42}$$

where n_d denotes the number of nodes, and n_d = 2, 3, and 4 is used for the linear, quadratic, and cubic elements, respectively.

The strain and stress components, the Lagrange multipliers, and the displacement continuity conditions are expressed in the matrix form as follows:

$$\begin{aligned}\left(\varepsilon_x^{(e)}\right)^{(m)} &= \left[\mathbf{B}_1^{(e)}\left(\psi_i^{(e)}\right)\right]^{(m)}\left(\mathbf{u}^{(e)}\right)^{(m)}, \left(\varepsilon_z^{(e)}\right)^{(m)} = \left[\mathbf{B}_2^{(e)}\left(\psi_i^{(e)}\right)\right]^{(m)}\left(\mathbf{w}^{(e)}\right)^{(m)}, \\ \left(\gamma_{xz}^{(e)}\right)^{(m)} &= \left[\mathbf{B}_2^{(e)}\left(\psi_i^{(e)}\right)\right]^{(m)}\left(\mathbf{u}^{(e)}\right)^{(m)} + \left[\mathbf{B}_1^{(e)}\left(\psi_i^{(e)}\right)\right]^{(m)}\left(\mathbf{w}^{(e)}\right)^{(m)}, \\ \left(\sigma_x^{(e)}\right)^{(m)} &= \left(Q_{11}^{(e)}\right)^{(m)}\left[\mathbf{B}_1^{(e)}\left(\psi_i^{(e)}\right)\right]^{(m)}\left(\mathbf{u}^{(e)}\right)^{(m)} + \left(Q_{13}^{(e)}\right)^{(m)}\left[\mathbf{B}_2^{(e)}\left(\psi_i^{(e)}\right)\right]^{(m)}\left(\mathbf{w}^{(e)}\right)^{(m)} - \left(Q_{1\alpha}^{(e)}\right)^{(m)}\Delta T, \\ \left(\sigma_z^{(e)}\right)^{(m)} &= \left(Q_{13}^{(e)}\right)^{(m)}\left[\mathbf{B}_1^{(e)}\left(\psi_i^{(e)}\right)\right]^{(m)}\left(\mathbf{u}^{(e)}\right)^{(m)} + \left(Q_{33}^{(e)}\right)^{(m)}\left[\mathbf{B}_1^{(e)}\left(\psi_i^{(e)}\right)\right]^{(m)}\left(\mathbf{w}^{(e)}\right)^{(m)} - \left(Q_{3\alpha}^{(e)}\right)^{(m)}\Delta T, \\ \left(\tau_{xz}^{(e)}\right)^{(m)} &= \left(Q_{55}^{(e)}\right)^{(m)}\left[\mathbf{B}_2^{(e)}\left(\psi_i^{(e)}\right)\right]^{(m)}\left(\mathbf{u}^{(e)}\right)^{(m)} + \left(Q_{55}^{(e)}\right)^{(m)}\left[\mathbf{B}_1^{(e)}\left(\psi_i^{(e)}\right)\right]^{(m)}\left(\mathbf{w}^{(e)}\right)^{(m)}, \\ \left(f_x^{(e)}\right)^{(m)} &= \left[\mathbf{B}_3^{(e)}\left(\psi_i^{(e)}\right)\right]^{(m)}\left(\mathbf{u}^{(e)}\right)^{(m)} + \left[\mathbf{B}_4^{(e)}\left(\psi_i^{(e)}\right)\right]^{(m)}\left(\mathbf{u}^{(e)}\right)^{(m+1)}, \\ \left(f_z^{(e)}\right)^{(m)} &= \left[\mathbf{B}_3^{(e)}\left(\psi_i^{(e)}\right)\right]^{(m)}\left(\mathbf{w}^{(e)}\right)^{(m)} + \left[\mathbf{B}_4^{(e)}\left(\psi_i^{(e)}\right)\right]^{(m)}\left(\mathbf{w}^{(e)}\right)^{(m+1)},\end{aligned} \tag{43}$$

where

$$\begin{aligned}\left[\mathbf{B}_1^{(e)}\left(\psi_i^{(e)}\right)\right]^{(m)} &= \left\{\begin{array}{cccc}\psi_{i,x}^{(e)} & z_m\,\psi_{i,x}^{(e)} & z_m^2\,\psi_{i,x}^{(e)} & z_m^3\,\psi_{i,x}^{(e)}\end{array}\right\}, \\ \left[\mathbf{B}_2^{(e)}\left(\psi_i^{(e)}\right)\right]^{(m)} &= \left\{\begin{array}{cccc}0 & \psi_i^{(e)} & 2z_m\,\psi_i^{(e)} & 3z_m^2\,\psi_i^{(e)}\end{array}\right\}, \\ \left[\mathbf{B}_3^{(e)}\left(\psi_i^{(e)}\right)\right]^{(m)} &= \left\{\begin{array}{cccc}-\psi_i^{(e)} & (-h_m/2)\,\psi_i^{(e)} & \left(-h_m^2/4\right)\psi_i^{(e)} & \left(-h_m^3/8\right)\psi_i^{(e)}\end{array}\right\}, \\ \left[\mathbf{B}_4^{(e)}\left(\psi_i^{(e)}\right)\right]^{(m)} &= \left\{\begin{array}{cccc}\psi_i^{(e)} & (-h_m/2)\,\psi_i^{(e)} & \left(h_m^2/4\right)\psi_i^{(e)} & \left(-h_m^3/8\right)\psi_i^{(e)}\end{array}\right\},\end{aligned}$$

$\left[\mathbf{u}^{(e)}\right]^{(m)} = \left\{ \left(u_0^{(e)}\right)_i^{(m)} \quad \left(u_1^{(e)}\right)_i^{(m)} \quad \left(u_2^{(e)}\right)_i^{(m)} \quad \left(u_3^{(e)}\right)_i^{(m)} \right\}^T$, and

$\left[\mathbf{w}^{(e)}\right]^{(m)} = \left\{ \left(w_0^{(e)}\right)_i^{(m)} \quad \left(w_1^{(e)}\right)_i^{(m)} \quad \left(w_2^{(e)}\right)_i^{(m)} \quad \left(w_3^{(e)}\right)_i^{(m)} \right\}^T$,

Substituting Equations (42) and (43) into Equation (41) yields

$$\sum_{m=1}^{n_l}\sum_{e=1}^{n_e}\left\{\begin{bmatrix} 0 & 0 & \mathbf{K}_{13}^{(e)} & 0 & 0 & 0 \\ 0 & 0 & 0 & \mathbf{K}_{24}^{(e)} & 0 & 0 \\ \mathbf{K}_{31}^{(e)} & 0 & \mathbf{K}_{33}^{(e)} & \mathbf{K}_{34}^{(e)} & \mathbf{K}_{35}^{(e)} & 0 \\ 0 & \mathbf{K}_{42}^{(e)} & \mathbf{K}_{43}^{(e)} & \mathbf{K}_{44}^{(e)} & 0 & \mathbf{K}_{46}^{(e)} \\ 0 & 0 & \mathbf{K}_{53}^{(e)} & 0 & 0 & 0 \\ 0 & 0 & 0 & \mathbf{K}_{64}^{(e)} & 0 & 0 \end{bmatrix}^{(m)} \begin{Bmatrix} \left(\lambda_x^{(e)}\right)^{(m-1)} \\ \left(\lambda_z^{(e)}\right)^{(m-1)} \\ \left(\mathbf{u}^{(e)}\right)^{(m)} \\ \left(\mathbf{w}^{(e)}\right)^{(m)} \\ \left(\lambda_x^{(e)}\right)^{(m)} \\ \left(\lambda_z^{(e)}\right)^{(m)} \end{Bmatrix} = \begin{Bmatrix} 0 \\ 0 \\ 0 \\ \mathbf{P}_z^{(e)} \\ 0 \\ 0 \end{Bmatrix}^{(m)} + \begin{Bmatrix} 0 \\ 0 \\ \mathbf{P}_{xt}^{(e)} \\ \mathbf{P}_{zt}^{(e)} \\ 0 \\ 0 \end{Bmatrix}^{(m)}\right\}, \tag{44}$$

where

$$\left[\mathbf{K}_{rs}^{(e)}\left(\psi_i^{(e)},\ \psi_j^{(e)}\right)\right]^{(m)} = \left\{\left[\mathbf{K}_{sr}^{(e)}\left(\psi_j^{(e)},\ \psi_i^{(e)}\right)\right]^{(m)}\right\}^T \ (r \text{ and } s = 1-6),$$

$$\left(\mathbf{K}_{13}^{(e)}\right)^{(m)} = \left(\mathbf{K}_{24}^{(e)}\right)^{(m)} = \int_{x_e}^{x_{e+1}}\left(h_m\,\psi_i^{(e)}\right)\left[\mathbf{B}_4^{(e)}\left(\psi_j^{(e)}\right)\right]^{(m)}dx\ ,$$

$$\left[\mathbf{K}_{33}^{(e)}\right]^{(m)} = \int_{x_e}^{x_{e+1}}\left[\left(\mathbf{Q}_a^{(e)}\right)^{(m)}\left(\psi_i^{(e)}{}_{,x}\right)\left(\psi_j^{(e)}{}_{,x}\right) + \left(\mathbf{Q}_b^{(e)}\right)^{(m)}\psi_i^{(e)}\psi_j^{(e)}\right]^{(m)}dx\ ,$$

$$\left(\mathbf{K}_{34}^{(e)}\right)^{(m)} = \int_{x_e}^{x_{e+1}}\left[\left(\mathbf{Q}_c^{(e)}\right)^{(m)}\left(\psi_i^{(e)}{}_{,x}\right)\psi_j^{(e)} + \left(\mathbf{Q}_d^{(e)}\right)^{(m)}\psi_i^{(e)}\left(\psi_j^{(e)}{}_{,x}\right)\right]^{(m)}dx\ ,$$

$$\left(\mathbf{K}_{35}^{(e)}\right)^{(m)} = \left(\mathbf{K}_{46}^{(e)}\right)^{(m)} = \int_{x_e}^{x_{e+1}}\left(h_m\,\psi_i^{(e)}\right)\left[\mathbf{B}_3^{(e)}\left(\psi_j^{(e)}\right)\right]^{(m)}dx\ ,$$

$$\left(\mathbf{K}_{44}^{(e)}\right)^{(m)} = \int_{x_e}^{x_{e+1}}\left[\left(\mathbf{Q}_e^{(e)}\right)^{(m)}\left(\psi_i^{(e)}{}_{,x}\right)\left(\psi_j^{(e)}{}_{,x}\right) + \left(\mathbf{Q}_f^{(e)}\right)^{(m)}\psi_i^{(e)}\psi_j^{(e)}\right]^{(m)}dx\ ,$$

$$\left(\lambda_x^{(e)}\right)^{(m)} = \left\{\left(\lambda_x^{(e)}\right)_i^{(m)}\right\}, \left(\lambda_z^{(e)}\right)^{(m)} = \left\{\left(\lambda_z^{(e)}\right)_i^{(m)}\right\},$$

$$\left(\mathbf{P}_z^{(e)}\right)^{(m)} = \delta_{mn_l}\int_{x_e}^{x_{e+1}}\bar{q}(x)\,\psi_i^{(e)}\left\{\ 1 \quad (h_m/2) \quad \left(h_m^2/4\right) \quad \left(h_m^3/8\right)\ \right\}^T dx\ ,$$

$$\left(\mathbf{P}_{xt}^{(e)}\right)^{(m)} = \int_{x_e}^{x_{e+1}}\int_{-h_m/2}^{h_m/2} Q_{1\alpha}^{(m)}\,(\Delta T)\left(\psi_i^{(e)}{}_{,x}\right)\left\{\ 1 \quad z_m \quad z_m^2 \quad z_m^3\ \right\}^T dz_m\,dx,$$

$$\left(\mathbf{P}_{zt}^{(e)}\right)^{(m)} = \int_{x_e}^{x_{e+1}}\int_{-h_m/2}^{h_m/2} Q_{3\alpha}^{(m)}\,(\Delta T)\left(\psi_i^{(e)}\right)\left\{\ 0 \quad 1 \quad 2z_m \quad 3z_m^2\ \right\}^T dz_m\,dx,$$

$$\left(\mathbf{Q}_a^{(e)}\right)^{(m)} = \begin{bmatrix} A_{11}^{(m)} & B_{11}^{(m)} & D_{11}^{(m)} & F_{11}^{(m)} \\ B_{11}^{(m)} & D_{11}^{(m)} & F_{11}^{(m)} & H_{11}^{(m)} \\ D_{11}^{(m)} & F_{11}^{(m)} & H_{11}^{(m)} & J_{11}^{(m)} \\ F_{11}^{(m)} & H_{11}^{(m)} & J_{11}^{(m)} & L_{11}^{(m)} \end{bmatrix}, \left(\mathbf{Q}_b^{(e)}\right)^{(m)} = \begin{bmatrix} 0 & 0 & 0 & 0 \\ 0 & A_{55}^{(m)} & 2B_{55}^{(m)} & 3D_{55}^{(m)} \\ 0 & 2B_{55}^{(m)} & 4D_{55}^{(m)} & 6F_{55}^{(m)} \\ 0 & 3D_{55}^{(m)} & 6F_{55}^{(m)} & 9H_{55}^{(m)} \end{bmatrix},$$

$$\left(\mathbf{Q}_c^{(e)}\right)^{(m)} = \begin{bmatrix} 0 & A_{13}^{(m)} & 2B_{13}^{(m)} & 3D_{13}^{(m)} \\ 0 & B_{13}^{(m)} & 2D_{13}^{(m)} & 3F_{13}^{(m)} \\ 0 & D_{13}^{(m)} & 2F_{13}^{(m)} & 3H_{13}^{(m)} \\ 0 & F_{13}^{(m)} & 2H_{13}^{(m)} & 3J_{13}^{(m)} \end{bmatrix}, \left(\mathbf{Q}_d^{(e)}\right)^{(m)} = \begin{bmatrix} 0 & 0 & 0 & 0 \\ A_{55}^{(m)} & B_{55}^{(m)} & D_{55}^{(m)} & F_{55}^{(m)} \\ 2B_{55}^{(m)} & 2D_{55}^{(m)} & 2F_{55}^{(m)} & 2H_{55}^{(m)} \\ 3D_{55}^{(m)} & 3F_{55}^{(m)} & 3H_{55}^{(m)} & 3J_{55}^{(m)} \end{bmatrix},$$

$$\left(\mathbf{Q}_e^{(e)}\right)^{(m)} = \begin{bmatrix} A_{55}^{(m)} & B_{55}^{(m)} & D_{55}^{(m)} & F_{55}^{(m)} \\ B_{55}^{(m)} & D_{55}^{(m)} & F_{55}^{(m)} & H_{55}^{(m)} \\ D_{55}^{(m)} & F_{55}^{(m)} & H_{55}^{(m)} & J_{55}^{(m)} \\ F_{55}^{(m)} & H_{55}^{(m)} & J_{55}^{(m)} & L_{55}^{(m)} \end{bmatrix}, \text{ and } \left(\mathbf{Q}_f^{(e)}\right)^{(m)} = \begin{bmatrix} 0 & 0 & 0 & 0 \\ 0 & A_{33}^{(m)} & 2B_{33}^{(m)} & 3D_{33}^{(m)} \\ 0 & 2B_{33}^{(m)} & 4D_{33}^{(m)} & 6F_{33}^{(m)} \\ 0 & 3D_{33}^{(m)} & 6F_{33}^{(m)} & 9H_{33}^{(m)} \end{bmatrix}.$$

The finite element solutions of the nodal displacement components and the nodal Lagrange multipliers can be obtained by solving Equation (44). The secondary field variables can thus be obtained using the determined primary nodal field variables.

5. Boundary Conditions

There are four boundary conditions considered in the following numerical examples, i.e., C–C, C–S, S–S, and C–F boundary conditions, which are given as follows:

For the C–C boundary conditions,

$$\begin{gathered} u_0^{(m)} = u_1^{(m)} = u_2^{(m)} = u_3^{(m)} = 0, w_0^{(m)} = w_1^{(m)} = w_2^{(m)} = w_3^{(m)} = 0, \\ \lambda_x^{(k)} = 0, \text{ and } \lambda_z^{(k)} = 0, \text{ at } x = 0 \text{ and } x = L. \end{gathered} \tag{45}$$

For the C–S boundary conditions,

$$u_0^{(m)} = u_1^{(m)} = u_2^{(m)} = u_3^{(m)} = 0, w_0^{(m)} = w_1^{(m)} = w_2^{(m)} = w_3^{(m)} = 0, \lambda_x^{(k)} = 0, \text{ and } \lambda_z^{(k)} = 0, \text{ at } x = 0; \tag{46}$$

$$N_x^{(m)} = M_x^{(m)} = P_x^{(m)} = R_x^{(m)} = 0, w_0^{(m)} = w_1^{(m)} = w_2^{(m)} = w_3^{(m)} = 0, \text{ and } \lambda_z^{(k)} = 0, \text{ at } x = L. \tag{47}$$

For the S–S boundary conditions,

$$N_x^{(m)} = M_x^{(m)} = P_x^{(m)} = R_x^{(m)} = 0, w_0^{(m)} = w_1^{(m)} = w_2^{(m)} = w_3^{(m)} = 0, \text{ and } \lambda_z^{(k)} = 0, \text{ at } x = L. \tag{48}$$

For the C–F boundary conditions,

$$u_0^{(m)} = u_1^{(m)} = u_2^{(m)} = u_3^{(m)} = 0, w_0^{(m)} = w_1^{(m)} = w_2^{(m)} = w_3^{(m)} = 0, \lambda_x^{(k)} = 0, \text{ and } \lambda_z^{(k)} = 0, \text{at } x = 0; \tag{49}$$

$$N_x^{(m)} = M_x^{(m)} = P_x^{(m)} = R_x^{(m)} = 0, \text{ and } N_{xz}^{(m)} = M_{xz}^{(m)} = P_{xz}^{(m)} = R_{xz}^{(m)} = 0, \text{ at } x = L. \tag{50}$$

6. Numerical Examples

Based on the above-mentioned strong and weak formulations, the authors can obtain the Navier-type analytical solutions for static problems of simply supported, multi-layered FG beams subjected to thermo-mechanical loads, as well as the FE numerical solutions for those of multi-layered FG beams under various boundary conditions, respectively. Some numerical examples are examined and discussed in the following sections.

6.1. Mechanical Loads

In this work, the static behavior of an FG beam under various boundary conditions subjected to a uniformly distributed mechanical load (i.e., $q(x) = q_0$) applied on the top surface of an FG beam is considered. The FG beam is composed of a two-phase composite material by mixing a metal material (aluminum) and a ceramic material (alumina) according to a power-law distribution of the volume fractions of the constituents through the thickness direction of the FG beam. The material properties of the aluminum and alumina materials are E_m = 70 GPa, υ_m = 0.3, and E_c = 380 GPa, υ_c = 0.3, respectively, where the subscripts m and c represent the metal (aluminum) and ceramic (alumina) materials. For comparison purposes, a set of dimensionless variables is defined as the same forms as those used in Thai and Vo [16], and can be given as follows:

$$\overline{u} = 100E_m h^3 u(0, -h/2)/\left(q_0 L^4\right), \overline{w} = 100E_m h^3 w(L/2, 0)/\left(q_0 L^4\right), \tag{51}$$

$$\overline{\sigma}_x = h\,\sigma_x(L/2, h/2)/(q_0 L), \overline{\tau}_{xz} = h\,\tau_{xz}(0, 0)/(q_0 L), \overline{\sigma}_z = h\,\sigma_z(L/2, 0)/(q_0 L).$$

The applied external load is expanded as the single Fourier series in the x direction as follows:

$$q_0 = \sum_{\hat{m}=1}^{\infty} q_{\hat{m}} \sin(m\,x), \quad (52)$$

where $q_{\hat{m}} = 4q_0/\left(\hat{m}\,\pi\right)$, when $\hat{m}$ is an odd integer, and $q_{\hat{m}} = 0$, when $\hat{m}$ is an even integer. In this example, $\hat{m}$ is taken as $\hat{m} = 1,\ 3, 5, \ldots, 39$ for a uniform mechanical load.

The volume fraction of the ceramic material $\Gamma_c(z)$ is defined as $\Gamma_c(z) = [(1/2) + (z/h)]^{\kappa_p}$, where κ_p denotes the material-property gradient index of a power-law-type material model. The effective material properties are estimated using the rule of mixtures, for which a formula is given as Equation (1).

In the mixed LW HSDT, the transverse shear and normal stress components induced in the loaded FG beams can be obtained using three different approaches. In approach 1, they are obtained using constitutive equations when the displacement components are determined. In approach 2, they are obtained using stress equilibrium equations when the displacement components are determined. In approach 3, they are directly obtained using the Lagrange multipliers.

Table 1 shows the convergent study for analytical solutions of the stress and displacement components induced in a simply supported, FG beam subjected to a uniform mechanical load, where L/h = 5 and 20, and L = 5 m; κ_p= 5; n_l = 4, 8, and 16 for the LW1, and n_l = 2, 4, and 8 for the LW2 and LW3 theories. LW1, LW2, and LW3 represent the mixed LW FSDT, the mixed LW second-order shear deformation, and the mixed LW TSDT, respectively. It can be seen in Table 1 that the convergent solutions are obtained when n_l is taken to be 16, 8, and 4, for the LW1, LW2, and LW3 theories, respectively. The convergence rates of LW1, LW2, and LW3 are in the following order: LW3 > LW2 > LW1, where the symbol ">" indicates a fast convergence rate. The convergent results for the LW1, LW2, and LW3 theories are also compared with the solutions obtained using the HSDT [33], RSDT [34], sinusoidal shear deformation theory (SSDT) [35], TSDT [36], exponential shear deformation theory (ESDT) [37], and classical beam theory (CBT) [16]. The results show that the convergent solutions of the displacement and in-plane stress components obtained using the mixed LW HSDT are in excellent agreement with those solutions obtained using the HSDT, RHSDT, SSDT, TSDT, and ESDT. The CBT fails to provide satisfactory results for the analysis of FG beams. It is well known that the transverse shear and normal stress components obtained using the stress equilibrium equation approach (i.e., approach 2) are significantly more accurate than those obtained using the constitutive equation approach (i.e., approach 1), although the solution process for the former is more complicated and more time consuming than that of the latter. In the LW HSDTs, the transverse shear stress components can also be directly obtained using the Lagrange multipliers (i.e., approach 3), which are the primary variables, without any additional processing procedures, and these components obtained using approach 3 closely agree with those obtained using approach 2. In most of the beam theories available in the literature, the transverse shear and normal stress components were obtained using the constitutive equation approach (i.e., approach 1), such that these components predicted by various theories are different from each other. On the basis of the convergent solutions for LW3, the relative errors for the transverse shear stress components obtained using the HSDT, RHSDT, SSDT, TSDT, and ESDT are 9.42%, 7.62%, 3.71%, 7.96%, and 0.19%, respectively, for thick beams (L/h = 5). The accuracy of the transverse shear stress components for various theories is in the following order: ESDT > SSDT > (RHSDT, TSDT) > HSDT, where the symbol ">" represents greater accuracy.

Table 1. Convergent study for analytical solutions of stress and displacement components induced in simply supported, FG beams under a mechanical load.

L/h	κ_p	Theories	$\bar{w}$ $(L/2, 0)$	$\bar{u}$ $(0, -h/2)$	$\bar{\sigma}_x$ $(L/2, h/2)$	$\bar{\tau}_{xz}(0,0)$			$\bar{\sigma}_z(L/2,0)$		
						Approach 1	Approach 2	Approach 3	Approach 1	Approach 2	Approach 3
5	5	Current L_1 (n_l = 4)	9.8459	3.6559	8.1050	0.5432	0.6346	0.6392	−0.0550	-0.0842	-0.0818
		Current L_1 (n_l = 8)	9.8461	3.6768	8.1471	0.6070	0.6380	0.6392	−0.0693	−0.0824	−0.0818
		Current L_1 (n_l = 16)	9.8462	3.6826	8.1551	0.6273	0.6389	0.6392	−0.0759	−0.0819	−0.0818
		Current L_2 (n_l = 2)	9.8444	3.6618	8.1498	0.7386	0.6427	0.6428	−0.0720	−0.0915	−0.0818
		Current L_2 (n_l = 4)	9.8460	3.6822	8.1635	0.6885	0.6392	0.6392	−0.0832	−0.0844	−0.0818
		Current L_2 (n_l = 8)	9.8463	3.6844	8.1588	0.6546	0.6392	0.6392	−0.0829	−0.0824	−0.0818
		Current L_3 (n_l = 2)	9.8456	3.6845	8.1581	0.6710	0.6428	0.6428	−0.0858	−0.0818	−0.0818
		Current L_3 (n_l = 4)	9.8463	3.6847	8.1571	0.6436	0.6392	0.6392	−0.0826	−0.0818	−0.0818
		Current L_3 (n_l = 8)	9.8463	3.6847	8.1565	0.6395	0.6392	0.6392	−0.0819	−0.0818	−0.0818
		HSDT [33]	9.7802	3.7089	8.1030	0.5790	NA	NA	NA	NA	NA
		RSDT [34]	9.8281	3.7100	8.1106	0.5905	NA	NA	NA	NA	NA
		SSDT [35]	9.8367	3.7140	8.1222	0.6155	NA	NA	NA	NA	NA
		TSDT [36]	9.8271	3.7097	8.1095	0.5883	NA	NA	NA	NA	NA
		ESDT [37]	9.8414	3.7177	8.1329	0.6404	NA	NA	NA	NA	NA
		CBT [16]	8.7508	3.6496	7.9428	NA	NA	NA	NA	NA	NA
20	5	Current L_1 (n_l = 4)	8.8197	0.9126	31.8104	0.5725	0.6704	0.6715	−0.0137	−0.0210	−0.0204
		Current L_1 (n_l = 8)	8.8197	0.9130	31.8209	0.6383	0.6712	0.6715	−0.0173	−0.0205	−0.0204
		Current L_1 (n_l = 16)	8.8197	0.9131	31.8233	0.6592	0.6714	0.6715	−0.0189	−0.0204	−0.0204
		Current L_2 (n_l = 2)	8.8197	0.9127	31.8219	0.7500	0.6715	0.6715	−0.0179	−0.0228	−0.0203
		Current L_2 (n_l = 4)	8.8197	0.9131	31.8250	0.7228	0.6715	0.6715	−0.0207	−0.0210	−0.0204
		Current L_2 (n_l = 8)	8.8197	0.9131	31.8242	0.6878	0.6715	0.6715	−0.0206	−0.0205	−0.0204
		Current L_3 (n_l = 2)	8.8197	0.9131	31.8240	0.7172	0.6715	0.6715	−0.0214	−0.0203	−0.0203
		Current L_3 (n_l = 4)	8.8197	0.9131	31.8241	0.6766	0.6715	0.6715	−0.0206	−0.0204	−0.0204
		Current L_3 (n_l = 8)	8.8197	0.9131	31.8241	0.6718	0.6715	0.6715	−0.0204	−0.0204	−0.0204
		HSDT [33]	8.8151	0.9133	31.8112	0.5790	NA	NA	NA	NA	NA
		RSDT [34]	8.8182	0.9134	31.8130	0.6023	NA	NA	NA	NA	NA
		SSDT [35]	8.8188	0.9134	31.8159	0.6292	NA	NA	NA	NA	NA
		TSDT [36]	8.8181	0.9134	31.8127	0.5998	NA	NA	NA	NA	NA
		ESDT [37]	8.8191	0.9135	31.8185	0.6562	NA	NA	NA	NA	NA
		CBT [16]	8.7508	0.9124	31.7711	NA	NA	NA	NA	NA	NA

Approach 1: solutions obtained using constitutive equations; approach 2: solutions obtained using stress equilibrium equations; approach 3: solutions obtained using the Lagrange multipliers. HSDT: higher-order shear deformation theory; RSDT: refined shear deformation theory; SSDT: sinusoidal shear deformation theory; TSDT: trigonometric shear deformation theory; ESDT: exponential shear deformation theory; CBT: classical shear deformation theory.

In order to expand the applicable range of the mixed LW HSDT to the analysis of FG beams under different boundary conditions, rather than under simply supported boundary conditions only, a weak formulation-based finite element method is developed in this work. As the results in Table 1 show that the performance of LW3 is superior to that of LW2 and LW1, an LW3-based quadratic finite element method is developed for the thermo-mechanical analysis of FG beams under combinations of simply supported, free, and clamped boundary conditions. Table 2 shows a convergent study for the LW3-based quadratic FEM solutions of stress and displacement components induced in the FG beam under various boundary conditions, including the C–C, C–S, S–S, and C–F boundary conditions, subjected to a uniform mechanical load. It can be seen in Table 2 that the convergent solutions for the stress and displacement components induced in the FG beam can be obtained using an element mesh $(n_x \times n_z) = (32 \times 16)$ for a wide range of $L/h > 5$, where n_x and n_z denote the numbers of elements used in the x and z directions, respectively. For a moderately thick FG beam ($L/h = 10$) and on the basis of an allowable relative error of 1%, the convergent solutions of displacement, in-plane stress, and transverse stress components can be obtained when $(n_x \times n_z) = (8 \times 16)$, (16×16), and (32×16) element meshes are used, respectively. The values of the displacement components u_x and u_z at some specific positions for assorted boundary conditions are in the following order: C–C < C–S < S–S < C–F, where the symbol "<" indicates a less displacement and greater gross beam stiffness.

Figures 2 and 3 show variations in the through-thickness distributions of various stress and displacement components induced in a simply supported FG beam under a uniform mechanical load with different L/h ratios and different values of material-property gradient indices, respectively, where the LW3 theory with $n_l = 32$ is used. In Figure 2, the length-to-thickness ratio is taken as $L/h = 5$, 10, and 20, and the material-property gradient index is taken as $\kappa_p = 3$. In Figure 3, they are $L/h = 10$, and $\kappa_p = 0$, 0.2, 5, and ∞.

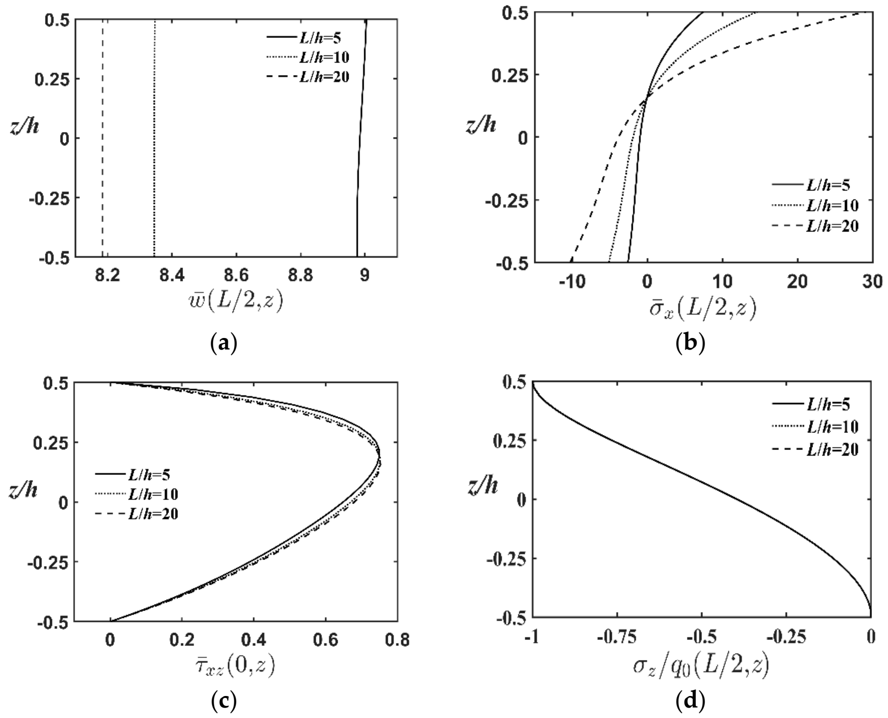

Figure 2. Variations in the through-thickness distributions of various stress and displacement components induced in an FG beam with different length–thickness ratios subjected to a uniform mechanical load: (**a**) the displacement component $\overline{w}$, (**b**) the in-plane normal stress component $\overline{\sigma}_x$, (**c**) the transverse shear stress component $\overline{\tau}_{xz}$, (**d**) the transverse normal stress component $\overline{\sigma}_z$, where $L/h = 5$, 10, and 20; $h = 0.01$ m and $\kappa_p = 3$.

Table 2. Convergent study for layer-wise (LW)3-based quadratic FEM solutions of stress and displacement components induced in an FG beam under various boundary conditions subjected to a uniform mechanical load. FEM: finite element methods.

L/h	κ_p	Boundary Conditions	Current LW3 FEM ($n_e \times n_l$) and Analytical Solutions	$\bar{w}$ ($L/2$, 0)	$\bar{u}$ ($L/4$, $-h/2$)	$\bar{\sigma}_x$ ($L/2$, $h/2$)	$\bar{\tau}_{xz}$ ($L/4$, 0)	$\bar{\sigma}_z$ ($L/4$, 0)
5	5	S–S	Current LW3 FEM (2 × 16)	9.3110	2.3283	8.0867	0.1956	−0.1040
			Current LW3 FEM (4 × 16)	9.8064	2.5412	8.3122	0.4350	−0.0762
			Current LW3 FEM (8 × 16)	9.8435	2.5341	8.2195	0.3667	−0.0822
			Current LW3 FEM (16 × 16)	9.8461	2.5329	8.1780	0.3479	−0.0825
			Current LW3 FEM (32 × 16)	9.8463	2.5327	8.1650	0.3434	−0.0825
			Current LW3 analytical solutions	9.8463	2.5326	8.1565	0.3419	−0.0825
10	5	C–C	Current LW3 FEM (2 × 16)	0.8045	0.1171	2.7839	0.1436	−0.0322
			Current LW3 FEM (4 × 16)	1.8644	0.3471	5.3558	0.5644	−0.0459
			Current LW3 FEM (8 × 16)	2.0049	0.3460	5.4767	0.4296	−0.0379
			Current LW3 FEM (16 × 16)	2.0190	0.3453	5.4335	0.3657	−0.0409
			Current LW3 FEM (32 × 16)	2.0206	0.3451	5.4128	0.3478	−0.0409
10	5	S–S	Current LW3 FEM (2 × 16)	7.9337	1.0465	13.4887	0.0036	−0.0663
			Current LW3 FEM (4 × 16)	8.9089	1.2609	15.9385	0.6858	−0.0119
			Current LW3 FEM (8 × 16)	9.0168	1.2585	16.0672	0.4423	−0.0386
			Current LW3 FEM (16 × 16)	9.0255	1.2577	16.0239	0.3662	−0.0409
			Current LW3 FEM (32 × 16)	9.0261	1.2575	16.0032	0.3478	−0.0409
			Current LW3 analytical solutions	9.0261	1.2575	15.9921	0.3417	−0.0409
10	5	C–S	Current LW3 FEM (2 × 16)	2.4077	0.3325	7.9771	0.1791	−0.0262
			Current LW3 FEM (4 × 16)	3.6503	0.6304	8.8481	0.8795	−0.0550
			Current LW3 FEM (8 × 16)	3.8062	0.6224	8.4294	0.6455	−0.0377
			Current LW3 FEM (16 × 16)	3.8211	0.6206	8.2202	0.5470	−0.0409
			Current LW3 FEM (32 × 16)	3.8226	0.6203	8.1529	0.5200	−0.0409
10	5	C–F	Current LW3 FEM (2 × 16)	27.1018	3.5694	7.7092	0.2246	0.0102
			Current LW3 FEM (4 × 16)	30.1461	4.2363	12.5271	1.8370	−0.0830
			Current LW3 FEM (8 × 16)	30.5292	4.2316	14.7599	1.3013	−0.0371
			Current LW3 FEM (16 × 16)	30.5660	4.2293	15.4893	1.0976	−0.0409
			Current LW3 FEM (32 × 16)	30.5698	4.2288	15.7002	1.0433	−0.0409

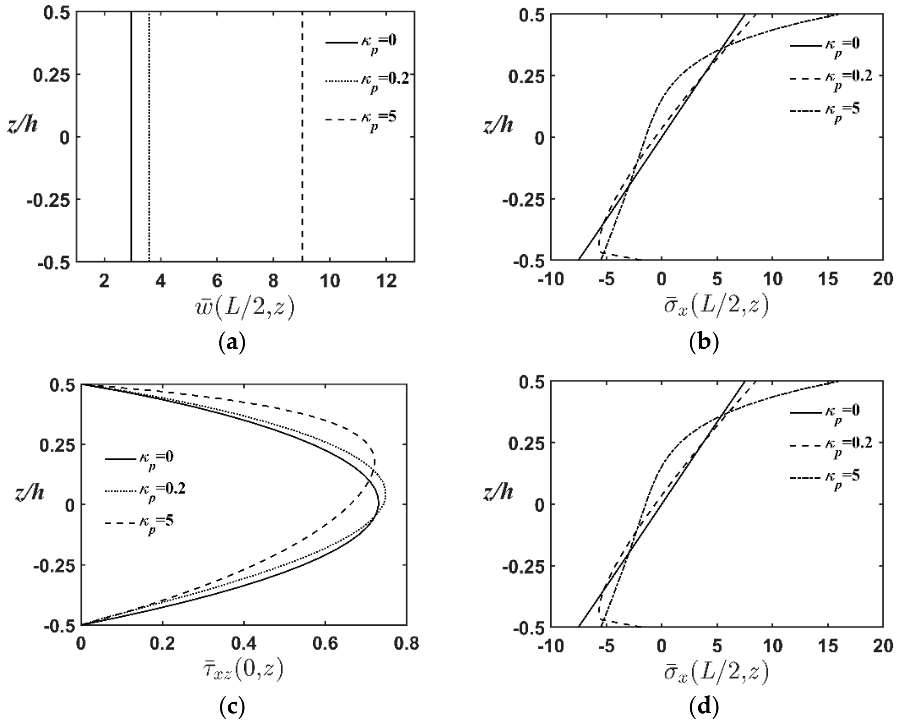

Figure 3. Variations in the through-thickness distributions of various stress and displacement components induced in an FG beam with different values of κ_p subjected to a uniform mechanical load: (**a**) the displacement component $\overline{w}$, (**b**) the in-plane normal stress component $\overline{\sigma}_x$, (**c**) the transverse shear stress component $\overline{\tau}_{xz}$, (**d**) the transverse normal stress component $\overline{\sigma}_z$, where κ_p = 0, 0.2, 5; h = 0.01 m and L/h = 10

A set of dimensionless variables is defined as follows:

$$\begin{gathered}\overline{u} = 100E_m h^3 u/\left(q_0 L^4\right), \overline{w} = 100E_m h^3 w/\left(q_0 L^4\right), \\ \overline{\sigma}_x = h\sigma_x/(q_0 L), \overline{\tau}_{xz} = h\,\tau_{xz}/(q_0 L), \overline{\sigma}_z = \sigma_z/q_0\end{gathered} \quad (53)$$

It can be seen in Figures 2b and 3b that the in-plane normal stress component σ_x induced in the FG beam increases when the FG beam becomes thinner, where $\kappa_p = 3$. It can also be seen that the through-thickness distribution of σ_x induced in the FG beam appears to be a higher-order polynomial function, $\kappa_p = 3$ and 5 rather than a linear function induced in an isotropic homogeneous beam (i.e., κ_p = 0). The results in Figure 2c and Figure 3c show that the through-thickness distribution of transverse shear stress component τ_{xz} appears to be a parabolic function for the isotropic homogeneous beam (i.e., κ_p = 0), where its peak value occurs in the mid-plane, and it appears to be a higher-order polynomial function with a peak value occurring at a position above half the beam height for the FG beam (i.e., $\kappa_p \neq 0$. Referring to the relationships of the dimensionless displacement component $\overline{w}$ to its dimensional counterpart w, it can be seen in Figures 2a and 3a that the displacement component w increases when the value of κ_p becomes greater, which indicates that the volume fraction of the metal material becomes greater than that of the ceramic material. In Figure 2c,d and Figure 3c,d, it is shown that the traction conditions on the top surface of the FG beam are exactly satisfied.

6.2. Thermal loads

In this section, the authors investigate the stress and deformation components induced in an FG beam under combinations of simply supported, free, and clamped boundary conditions subjected to a sinusoidally distributed thermal load using the strong and weak formulations of the mixed LW HSDTs. For comparison purposes, a numerical example used in Lü et al. [31] is adopted to validate the accuracy and convergence rate of the strong formulation-based analytical solutions and the weak formulation-based finite element solutions. In this example, the length and thickness of the FG beam are taken as $L = 0.1$ m and $h = 0.01$ m, respectively. The Young's modulus, Poisson's ratio, thermomechanical coefficients, and temperature changes are defined as

$$E(x, z) = E_0\, e^{\kappa_e[z+(h/2)]}, \tag{54}$$

$$\upsilon(x, z) = 0.25, \tag{55}$$

$$Q_{1\alpha}^{(m)} = Q_{3\alpha}^{(m)} = Q_{\alpha 0}, \tag{56}$$

$$\Delta T = T_0\, \sin(\pi x/L) e^{\kappa_e[z+(h/2)]}, \tag{57}$$

where E_0,, $Q_{\alpha 0}$, and T_0 denote a reference modulus, a reference thermomechanical coefficient, and a reference temperature change, respectively; $Q_{\alpha 0} = 10^{-6} E_0/(1 - \upsilon)$, and $T_0 = 100$ K κ_e stands for the material-property gradient index of an exponential function-type material model.

A set of dimensionless displacement and stress components is defined as having the same form as that used in Lü et al. [31] and can be given as follows:

$$\overline{w} = w/h, \tag{58}$$

$$(\overline{\sigma}_x,\ \overline{\tau}_{xz}, \overline{\sigma}_z) = (\sigma_x,\ \tau_{xz}, \sigma_z)/(T_0\, Q_{\alpha 0}), \tag{59}$$

Table 3 shows the convergent study for analytical solutions of thermal stress and thermal displacement components induced in a simply supported, FG beam subjected to a sinusoidally distributed thermal load, where $\kappa_e = 230$ and 100; $h/L = 0.1$ and 0.2, and $L = 0.1$ m; n_l= 16, 32, and 64 for the LW1 theory, n_l = 8, 16, and 32 for the LW2 theory, and n_l = 4, 8, and 16 for the LW3 theory. It can be seen in Table 3 that the convergent solutions are obtained when n_l is taken to be 32, 16, and 8, for the LW1, LW2, and LW3 theories, respectively. Again, the convergence rates of the LW1, LW2, and LW3 are in the following order: LW3 > LW2 > LW1, where the symbol ">" indicates a fast convergence rate. The convergent results of the LW1, LW2, and LW3 theories are also compared with the solutions obtained using a 13-node state space-based differential quadrature method (SSDQM) [31] and a bilinear rectangular plane element method (BRPEM) with an element mesh $(n_x \times n_z) = (200 \times 20)$ [31]. The results show that the convergent solutions of the displacement and in-plane stress components obtained using the mixed LW HSDT are in excellent agreement with those solutions obtained using the SSDQM and the BRPEM. Table 4 shows the convergent study for LW3-based quadratic FEM solutions for the stress and displacement components induced in an FG beam under various boundary conditions, where $\kappa_e = 230$ and 100; $h/L = 0.1$, and $(n_x \times n_z) = (16 \times 4)$, (32×8), (64×8), (128×8), and (256×8). It can be seen in Table 4 that the convergent solutions are obtained when the $(n_x \times n_z) = (256 \times 8)$ element mesh is used.

Table 3. Convergent study for the analytical solutions of stress and displacement components induced in a simply supported, FG beam under a sinusoidally distributed thermal load.

h/L	κ_e	Theories	$10^3\ \bar{w}$ $(L/2, -h/2)$	$\bar{\sigma}_x$ $(L/2, -h/2)$	$100\bar{\tau}_{xz}(0, 0)$			$\bar{\sigma}_z(L/2, 0)$		
					Approach 1	Approach 2	Approach 3	Approach 1	Approach 2	Approach 3
0.1	230	Current LW1 (n_l = 16)	9.7662	−1.5544	1.6977	6.5887	6.5590	0.5622	0.0114	0.0113
		Current LW1 (n_l = 32)	9.7662	−1.5564	4.1835	6.5664	6.5590	0.2802	0.0113	0.0113
		Current LW1 (n_l = 64)	9.7662	−1.5573	5.3849	6.5609	6.5590	0.1441	0.0113	0.0113
		Current LW2 (n_l = 8)	9.7662	−1.5610	6.9982	6.6113	6.5590	−0.1047	0.0116	0.0113
		Current LW2 (n_l = 16)	9.7662	−1.5588	6.6732	6.5721	6.5590	−0.0159	0.0113	0.0113
		Current LW2 (n_l = 32)	9.7662	−1.5593	6.5882	6.5623	6.5590	0.0047	0.0113	0.0113
		Current LW3 (n_l = 4)	9.7662	−1.5576	6.6304	6.5590	6.5590	0.0344	0.0113	0.0113
		Current LW3 (n_l = 8)	9.7662	−1.5580	6.5693	6.5590	6.5590	0.0137	0.0113	0.0113
		Current LW3 (n_l = 16)	9.7662	−1.5581	6.5604	6.5590	6.5590	0.0115	0.0113	0.0113
		SSDQM [31]	9.9772	−1.5648	6.6004	NA	NA	NA	NA	NA
		FEM [31]	9.7944	−1.5573	6.0427	NA	NA	NA	NA	NA
0.2	230	Current LW1 (n_l = 16)	33.316	−41.037	1.1403×10^3	1.4261×10^3	1.4255×10^3	9.5825	2.4869	2.4720
		Current LW1 (n_l = 32)	33.315	−40.968	1.2850×10^3	1.4256×10^3	1.4255×10^3	5.7645	2.4757	2.4720
		Current LW1 (n_l = 64)	33.315	−40.930	1.3558×10^3	1.4255×10^3	1.4255×10^3	4.0550	2.4729	2.4720
		Current LW2 (n_l = 8)	33.315	−40.901	1.4451×10^3	1.4277×10^3	1.4255×10^3	−2.7201	2.5045	2.4720
		Current LW2 (n_l = 16)	33.315	−40.893	1.4308×10^3	1.4260×10^3	1.4255×10^3	1.3386	2.4800	2.4720
		Current LW2 (n_l = 32)	33.315	−40.890	1.4269×10^3	1.4256×10^3	1.4255×10^3	2.2068	2.4740	2.4720
		Current LW3 (n_l = 4)	33.315	−40.887	1.4312×10^3	1.4255×10^3	1.4255×10^3	5.2356	2.4720	2.4720
		Current LW3 (n_l = 8)	33.315	−40.889	1.4265×10^3	1.4255×10^3	1.4255×10^3	2.7039	2.4720	2.4720
		Current LW3 (n_l = 16)	33.315	−40.889	1.4256×10^3	1.4255×10^3	1.4255×10^3	2.4959	2.4720	2.4720
0.1	100	Current LW1 (n_l = 16)	1.6955	−0.1008	−0.7732	0.1256	0.1226	0.0688	0.0005	0.0005
		Current LW1 (n_l = 32)	1.6956	−0.1035	−0.3189	0.1233	0.1226	0.0343	0.0005	0.0005
		Current LW1 (n_l = 64)	1.6956	−0.1048	−0.0966	0.1228	0.1226	0.0173	0.0005	0.0005
		Current LW2 (n_l = 8)	1.6956	−0.1066	0.1724	0.1269	0.1226	−0.0050	0.0005	0.0005
		Current LW2 (n_l = 16)	1.6956	−0.1062	0.1352	0.1236	0.1226	−0.0008	0.0005	0.0005
		Current LW2 (n_l = 32)	1.6956	−0.1062	0.1257	0.1228	0.1226	0.0002	0.0005	0.0005
		Current LW3 (n_l = 4)	1.6956	−0.1061	0.1257	0.1226	0.1226	0.0009	0.0005	0.0005
		Current LW3 (n_l = 8)	1.6956	−0.1061	0.1230	0.1226	0.1226	0.0005	0.0005	0.0005
		Current LW3 (n_l = 16)	1.6956	−0.1061	0.1226	0.1226	0.1226	0.0005	0.0005	0.0005

Approach 1: solutions obtained using constitutive equations; approach 2: solutions obtained using stress equilibrium equations; approach 3: solutions obtained using the Lagrange multipliers. SSDQM: state space differential quadrature method; FEM: finite element method.

Table 4. Convergent study for LW3-based quadratic FEM solutions of stress and displacement components induced in an FG beam under various boundary conditions subjected to a sinusoidally distributed thermal load.

κ_e	Boundary Conditions	Current LW3 FEM ($n_x \times n_z$) and Analytical Solutions	$10^3\ \bar{w}(L/2, -h/2)$	$\bar{\sigma}_x(L/2, -h/2)$	$100\bar{\tau}_{xz}(L/4, 0)$
230	S–S	Current LW3 FEM (16 × 4)	9.7651	−1.5573	11.1888
		Current LW3 FEM (32 × 8)	9.7661	−1.5584	6.2978
		Current LW3 FEM (64 × 8)	9.7662	−1.5582	5.0544
		Current LW3 FEM (128 × 8)	9.7662	−1.5581	4.7425
		Current LW3 FEM (256 × 8)	9.7662	−1.5581	4.6729
		Current LW3 analytical solutions	9.7662	−1.5581	4.6379
100	C–C	Current LW3 FEM (16 × 4)	0.2911	−0.5075	0.7075
		Current LW3 FEM (32 × 8)	0.2920	−0.5096	0.2412
		Current LW3 FEM (64 × 8)	0.2923	−0.5100	0.1254
		Current LW3 FEM (128 × 8)	0.2924	−0.5101	0.0963
		Current LW3 FEM (256 × 8)	0.2924	−0.5101	0.0890
100	S–S	Current LW3 FEM (16 × 4)	1.6954	−0.1036	0.6970
		Current LW3 FEM (32 × 8)	1.6956	−0.1055	0.2413
		Current LW3 FEM (64 × 8)	1.6956	−0.1060	0.1255
		Current LW3 FEM (128 × 8)	1.6956	−0.1061	0.0964
		Current LW3 FEM (256 × 8)	1.6956	−0.1061	0.0884
		Current LW3 analytical solutions	1.6956	−0.1061	0.0867
100	C–S	Current LW3 FEM (16 × 4)	0.6607	0.2565	3.4814
		Current LW3 FEM (32 × 8)	0.6614	0.2559	2.8198
		Current LW3 FEM (64 × 8)	0.6616	0.2558	2.6534
		Current LW3 FEM (128 × 8)	0.6617	0.2558	2.6117
		Current LW3 FEM (256 × 8)	0.6617	0.2558	2.6009
100	C–F	Current LW3 FEM (16 × 4)	−1.0853	−0.1036	0.6973
		Current LW3 FEM (32 × 8)	−1.0850	−0.1055	0.2413
		Current LW3 FEM (64 × 8)	−1.0850	−0.1060	0.1255
		Current LW3 FEM (128 × 8)	−1.0850	−0.1061	0.0964
		Current LW3 FEM (256 × 8)	−1.0850	−0.1061	0.0892

Figures 4 and 5 show variations in the through-thickness distributions of various stress and displacement components induced in a simply supported FG beam under a sinusoidally distributed thermal load with different L/h ratios and different values of material-property gradient indices, respectively, where the LW3 theory with $n_l = 32$ is used. In Figure 4, the length-to-thickness ratio is taken as $L/h = 5$, 10, and 20, and $h = 0.01$m, and the material-property gradient index is taken as $\kappa_e = 230$. In Figure 5, they are $L/h = 10$, and $\kappa_e = 0$, 200, and 300. A set of dimensionless variables is defined as those given in Equations (58) and (59). It can be seen in Figure 4a that the displacement component $\overline{w}$ induced in the FG beam increases when the FG beam becomes thinner, and in Figure 5a that it increases when the values of κ_e become greater, which indicates the FG beam becomes softer. A comparison of the results shown in Figure 2c,d and Figure 3c,d with those in Figure 4c,d and Figure 5c,d shows that the variations in the through-thickness distributions of the transverse shear and normal stresses with the length–thickness ratio and the material-property gradient index for the thermal load cases are more drastic than the variations for the mechanical load cases. Again, the results in Figure 4c,d and Figure 5c,d show that the through-thickness distribution of the transverse shear and normal stress components τ_{xz} and σ_z appear to be a higher-order polynomial function and that the traction conditions on the top surface of the FG beam are exactly satisfied.

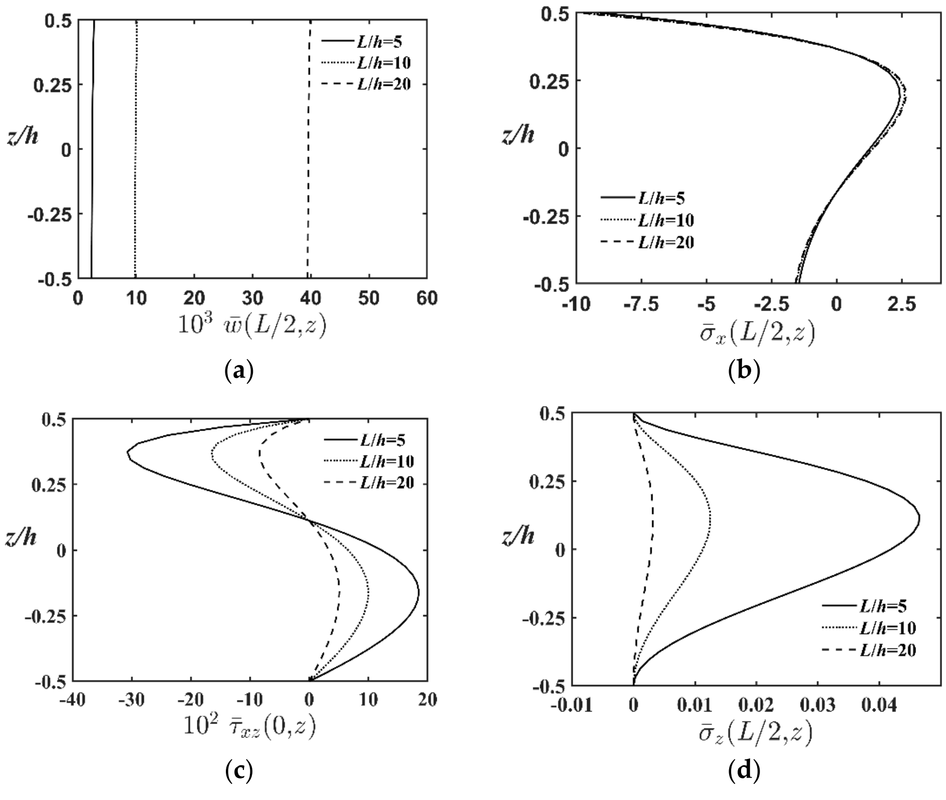

Figure 4. Variations in the through-thickness distributions of various stress and displacement components induced in an FG beam with different length–thickness ratios subjected to a sinusoidally distributed thermal load: (**a**) the displacement component $\overline{w}$, (**b**) the in-plane normal stress component $\overline{\sigma}_x$, (**c**) the transverse shear stress component $\overline{\tau}_{xz}$, (**d**) the transverse normal stress component $\overline{\sigma}_z$, where $L/h = 5$, 10, and 20; $h = 0.01$ m and $\kappa_e = 230$.

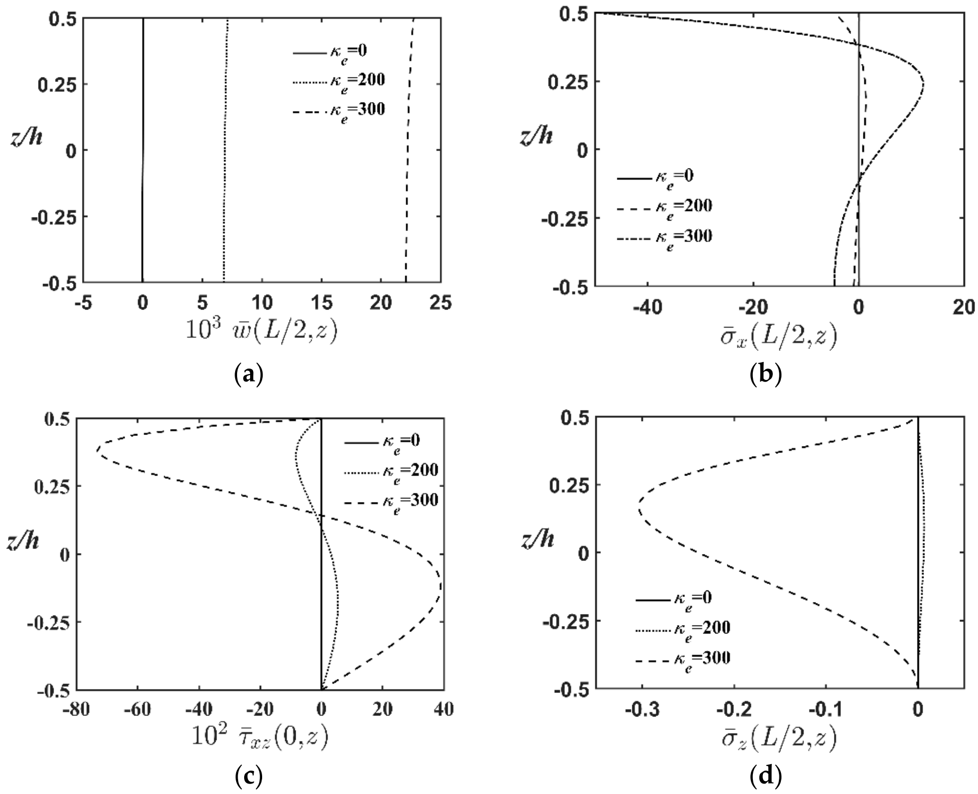

Figure 5. Variations in the through-thickness distributions of various stress and displacement components induced in an FG beam with different values of κ_e subjected to a sinusoidally distributed thermal load: (**a**) the displacement component $\overline{w}$, (**b**) the in-plane normal stress component $\overline{\sigma}_x$, (**c**) the transverse shear stress component $\overline{\tau}_{xz}$, (**d**) the transverse normal stress component $\overline{\sigma}_z$, where κ_e = 0, 200, and 300; h = 0.01 m and L/h = 10.

7. Concluding Remarks

In this work, the authors develop the strong and weak formulations of a mixed LW HSDT for the analysis of FG beams under various boundary conditions subjected to thermo-mechanical loads, where power-law-type and exponential function-type material models are considered and the rule of mixtures is used to estimate the effective material properties of the FG beams. In the numerical examples, the strong formulation-based Navier-type analytical solutions and the weak formulation-based FEM solutions are presented. The novelty of the LW HSDT is its displacement model can capture the 3D behavior of laminated FRC and multi-layered FG beams under different boundary conditions, including the zig-zag behavior of displacement components induced in laminated FRC beams and higher-order polynomial function distributions of displacement components induced in multi-layered FG beams. The transverse shear and normal stress components induced in laminated FRC and multi-layered FG beams can be obtained using the Lagrange multipliers, which are the primary variables in the current formulation and are much more accurate than those obtained using the constitutive equations approach that has been adopted by most of the displacement-based formulations available in the literature.

Some conclusions can be summarized as follows:

1. In the LW HSDT, the transverse shear and normal stress components induced in the thermo-mechanically loaded FG beams can be obtained using three different approaches. In approach 1, they are obtained using constitutive equations when the displacement components are determined; in approach 2, they are obtained using stress equilibrium equations when the displacement components are determined; in approach 3, they are directly obtained using the Lagrange multipliers. Implementation of the three approaches shows that the accuracy of these

approaches is in the following order: approach 2 > approach 3 > approach 1, where the symbol ">" indicates a greater degree of accuracy.

2. The accuracy and convergence rates of the LW1, LW2, and LW3 theories are in the following order: LW3 > LW2 > LW1, where the symbol ">" indicates a faster convergence rate and a more accurate solution.
3. Variations in the through-thickness distributions of the transverse shear and normal stresses with the length–thickness ratio and the material-property gradient index for the thermal load cases are more drastic than the variations for the mechanical load cases.
4. Based on the convergent solutions of the LW HSDT, the accuracy of the various advanced and refined beam theories is in the following order: ESDT > SSDT > (RHSDT, TSDT) > HSDT, where the symbol ">" represents a greater degree of accuracy.

Author Contributions: Conceptualization, C.-P.W.; methodology, C.-P.W.; software, Z.-R.X.; validation, C.-P.W. and Z.-R.X.; investigation: C.-P.W. and Z.-R.X.; resources, C.-P.W.; data curation, Z.-R.X.; writing—original draft preparation, C.-P.W.; writing—review and editing, C.-P.W.; visualization, C.-P.W.; supervision, C.-P.W.; project administration, C.-P.W.; funding acquisition, C.-P.W. All authors have read and agreed to the published version of the manuscript.

Funding: This research was funded by the Ministry of Science and Technology, Taiwan, grant number MOST 109-2221-E-006-015-MY3.

Conflicts of Interest: The authors declare no conflict of interest.

Appendix A. Relationships between the Resultant Forces/Moments and the Displacement Components

The relationships between the resultant forces/moments and the displacement components in the current mixed LW HSDT are given as follows:

$$N_x^{(m)} = A_{11}^{(m)} u_0^{(m)},_x + B_{11}^{(m)} u_1^{(m)},_x + D_{11}^{(m)} u_2^{(m)},_x + F_{11}^{(m)} u_3^{(m)},_x + A_{13}^{(m)} w_1^{(m)} + 2B_{13}^{(m)} w_2^{(m)} + 3D_{13}^{(m)} w_3^{(m)}, \tag{A1}$$

$$M_x^{(m)} = B_{11}^{(m)} u_0^{(m)},_x + D_{11}^{(m)} u_1^{(m)},_x + F_{11}^{(m)} u_2^{(m)},_x + H_{11}^{(m)} u_3^{(m)},_x + B_{13}^{(m)} w_1^{(m)} + 2D_{13}^{(m)} w_2^{(m)} + 3F_{13}^{(m)} w_3^{(m)}, \tag{A2}$$

$$P_x^{(m)} = D_{11}^{(m)} u_0^{(m)},_x + F_{11}^{(m)} u_1^{(m)},_x + H_{11}^{(m)} u_2^{(m)},_x + J_{11}^{(m)} u_3^{(m)},_x + D_{13}^{(m)} w_1^{(m)} + 2F_{13}^{(m)} w_2^{(m)} + 3H_{13}^{(m)} w_3^{(m)}, \tag{A3}$$

$$R_x^{(m)} = F_{11}^{(m)} u_0^{(m)},_x + H_{11}^{(m)} u_1^{(m)},_x + J_{11}^{(m)} u_2^{(m)},_x + L_{11}^{(m)} u_3^{(m)},_x + F_{13}^{(m)} w_1^{(m)} + 2H_{13}^{(m)} w_2^{(m)} + 3J_{13}^{(m)} w_3^{(m)}, \tag{A4}$$

$$N_z^{(m)} = A_{13}^{(m)} u_0^{(m)},_x + B_{13}^{(m)} u_1^{(m)},_x + D_{13}^{(m)} u_2^{(m)},_x + F_{13}^{(m)} u_3^{(m)},_x + A_{33}^{(m)} w_1^{(m)} + 2B_{33}^{(m)} w_2^{(m)} + 3D_{33}^{(m)} w_3^{(m)}, \tag{A5}$$

$$M_z^{(m)} = B_{13}^{(m)} u_0^{(m)},_x + D_{13}^{(m)} u_1^{(m)},_x + F_{13}^{(m)} u_2^{(m)},_x + H_{13}^{(m)} u_3^{(m)},_x + B_{33}^{(m)} w_1^{(m)} + 2D_{33}^{(m)} w_2^{(m)} + 3F_{33}^{(m)} w_3^{(m)}, \tag{A6}$$

$$P_z^{(m)} = D_{13}^{(m)} u_0^{(m)},_x + F_{13}^{(m)} u_1^{(m)},_x + H_{13}^{(m)} u_2^{(m)},_x + J_{13}^{(m)} u_3^{(m)},_x + D_{33}^{(m)} w_1^{(m)} + 2F_{33}^{(m)} w_2^{(m)} + 3H_{33}^{(m)} w_3^{(m)}, \tag{A7}$$

$$N_{xz}^{(m)} = A_{55}^{(m)} \left(w_0^{(m)},_x + u_1^{(m)}\right) + B_{55}^{(m)} \left(w_1^{(m)},_x + 2u_2^{(m)}\right) + D_{55}^{(m)} \left(w_2^{(m)},_x + 3\,u_3^{(m)}\right) + F_{55}^{(m)} w_3^{(m)},_x, \tag{A8}$$

$$M_{xz}^{(m)} = B_{55}^{(m)} \left(w_0^{(m)},_x + u_1^{(m)}\right) + D_{55}^{(m)} \left(w_1^{(m)},_x + 2u_2^{(m)}\right) + F_{55}^{(m)} \left(w_2^{(m)},_x + 3\,u_3^{(m)}\right) + H_{55}^{(m)} w_3^{(m)},_x, \tag{A9}$$

$$P_{xz}^{(m)} = D_{55}^{(m)} \left(w_0^{(m)},_x + u_1^{(m)}\right) + F_{55}^{(m)} \left(w_1^{(m)},_x + 2u_2^{(m)}\right) + H_{55}^{(m)} \left(w_2^{(m)},_x + 3\,u_3^{(m)}\right) + J_{55}^{(m)} w_3^{(m)},_x, \tag{A10}$$

$$R_{xz}^{(m)} = F_{55}^{(m)} \left(w_0^{(m)},_x + u_1^{(m)}\right) + H_{55}^{(m)} \left(w_1^{(m)},_x + 2u_2^{(m)}\right) + J_{55}^{(m)} \left(w_2^{(m)},_x + 3\,u_3^{(m)}\right) + L_{55}^{(m)} w_3^{(m)},_x, \tag{A11}$$

Appendix B. The Solution Process of the Fourier Series Expansion Method

The applied thermal and mechanical loads are expanded as follows:

$$q(x) = \sum_{\hat{m}=1}^{\infty} q_{\hat{m}} \sin(\overline{m}x), \tag{A12}$$

$$\Delta T(x, z) = \sum_{\hat{m}=1}^{\infty} \Delta T_{\hat{m}}(z) \sin(\overline{m}x), \tag{A13}$$

where $\overline{m} = \hat{m}\,\pi/L$ in which $\hat{m}$ represents the half-wave number in the x direction and is a positive integer.

By satisfying the simply supported boundary conditions, various field variables of the mth-layer are thus expanded as

$$u_i^{(m)} = \sum_{\hat{m}=1}^{\infty} u_{i\,\hat{m}}^{(m)} \cos(\overline{m}\,x), \tag{A14}$$

$$w_i^{(m)} = \sum_{\hat{m}=1}^{\infty} w_{i\,\hat{m}}^{(m)} \sin(\overline{m}\,x), \tag{A15}$$

$$\lambda_x^{(m)} = \sum_{\hat{m}=1}^{\infty} \lambda_{x\,\hat{m}}^{(m)} \cos(\overline{m}\,x), \tag{A16}$$

$$\lambda_z^{(m)} = \sum_{\hat{m}=1}^{\infty} \lambda_{z\,\hat{m}}^{(m)} \sin(\overline{m}\,x), \tag{A17}$$

where the subscript i = 0, 1, 2, and 3; m = 1, 2, . . . , n_l, and k = 1, 2, . . . , $(n_l - 1)$.

Substituting Equations (A14)–(A15) in the Euler–Lagrange equations (i.e., Equations (31)–(40)), the authors obtain

$$\begin{aligned}\delta u_0^{(m)} :\ & \overline{m}^2 A_{11}^{(m)} u_{0\hat{m}}^{(m)} + \overline{m}^2 B_{11}^{(m)} u_{1\hat{m}}^{(m)} + \overline{m}^2 D_{11}^{(m)} u_{2\hat{m}}^{(m)} + \overline{m}^2 F_{11}^{(m)} u_{3\hat{m}}^{(m)} - \overline{m}\, A_{13}^{(m)} w_{1\hat{m}}^{(m)} \\ & -2\overline{m}\, B_{13}^{(m)} w_{2\hat{m}}^{(m)} - 3\overline{m}\, D_{13}^{(m)} w_{3\hat{m}}^{(m)} + \left(\lambda_{x\hat{m}}^{(m-1)} - \lambda_{x\hat{m}}^{(m)}\right) = -\overline{m}\, N_{xt\hat{m}}^{(m)},\end{aligned} \tag{A18}$$

$$\begin{aligned}\delta u_1^{(m)} :\ & \overline{m}^2 B_{11}^{(m)} u_{0\hat{m}}^{(m)} + \left(\overline{m}^2 D_{11}^{(m)} + A_{55}^{(m)}\right) u_{1\hat{m}}^{(m)} + \left(\overline{m}^2 F_{11}^{(m)} + 2B_{55}^{(m)}\right) u_{2\hat{m}}^{(m)} \\ & + \left(\overline{m}^2 H_{11}^{(m)} + 3D_{55}^{(m)}\right) u_{3\hat{m}}^{(m)} + \overline{m} A_{55}^{(m)} w_{0\hat{m}}^{(m)} + \left(-mB_{13}^{(m)} + mB_{55}^{(m)}\right) w_{1\hat{m}}^{(m)} + \left(-2mD_{13}^{(m)} + mD_{55}^{(m)}\right) w_{2\hat{m}}^{(m)} \\ & + \left(-3mF_{13}^{(m)} + mF_{55}^{(m)}\right) w_{3\hat{m}}^{(m)} + (-h_m/2)\left(\lambda_{x\hat{m}}^{(m-1)} + \lambda_{x\hat{m}}^{(m)}\right) = -\overline{m}\, M_{xt\hat{m}}^{(m)},\end{aligned} \tag{A19}$$

$$\begin{aligned}\delta u_2^{(m)} :\ & \overline{m}^2 D_{11}^{(m)} u_{0\hat{m}}^{(m)} + \left(\overline{m}^2 F_{11}^{(m)} + 2B_{55}^{(m)}\right) u_{1\hat{m}}^{(m)} + \left(\overline{m}^2 H_{11}^{(m)} + 4D_{55}^{(m)}\right) u_{2\hat{m}}^{(m)} \\ & + \left(\overline{m}^2 J_{11}^{(m)} + 6F_{55}^{(m)}\right) u_{3\hat{m}}^{(m)} + 2\overline{m} B_{55}^{(m)} w_{0\hat{m}}^{(m)} + \left(-mD_{13}^{(m)} + 2mD_{55}^{(m)}\right) w_{1\hat{m}}^{(m)} + \left(-2mF_{13}^{(m)} + 2mF_{55}^{(m)}\right) w_{2\hat{m}}^{(m)} \\ & + \left(-3mH_{13}^{(m)} + 2mH_{55}^{(m)}\right) w_{3\hat{m}}^{(m)} + \left(h_m^2/4\right)\left(\lambda_{x\hat{m}}^{(m-1)} + \lambda_{x\hat{m}}^{(m)}\right) = -\overline{m}\, P_{xt\hat{m}}^{(m)},\end{aligned} \tag{A20}$$

$$\begin{aligned}\delta u_3^{(m)} :\ & \overline{m}^2 F_{11}^{(m)} u_{0\hat{m}}^{(m)} + \left(\overline{m}^2 H_{11}^{(m)} + 3D_{55}^{(m)}\right) u_{1\hat{m}}^{(m)} + \left(\overline{m}^2 J_{11}^{(m)} + 6F_{55}^{(m)}\right) u_{2\hat{m}}^{(m)} \\ & + \left(\overline{m}^2 L_{11}^{(m)} + 9H_{55}^{(m)}\right) u_{3\hat{m}}^{(m)} + 3\overline{m} D_{55}^{(m)} w_{0\hat{m}}^{(m)} + \left(-mF_{13}^{(m)} + 3mF_{55}^{(m)}\right) w_{1\hat{m}}^{(m)} + \left(-2mH_{13}^{(m)} + 3mH_{55}^{(m)}\right) w_{2\hat{m}}^{(m)} \\ & + \left(-3mJ_{13}^{(m)} + 3mJ_{55}^{(m)}\right) w_{3\hat{m}}^{(m)} + \left(-h_m^3/8\right)\left(\lambda_{x\hat{m}}^{(m-1)} + \lambda_{x\hat{m}}^{(m)}\right) = -\overline{m}\, R_{xt\hat{m}}^{(m)},\end{aligned} \tag{A21}$$

$$\begin{aligned}\delta w_0^{(m)} :\ & \overline{m} A_{55}^{(m)} u_{1\hat{m}}^{(m)} + 2\overline{m}\, B_{55}^{(m)} u_{2\hat{m}}^{(m)} + 3\overline{m}\, D_{55}^{(m)} u_{3\hat{m}}^{(m)} + \overline{m}^2 A_{55}^{(m)} w_{0\hat{m}}^{(m)} + \overline{m}^2 B_{55}^{(m)} w_{1\hat{m}}^{(m)} \\ & + \overline{m}^2 D_{55}^{(m)} w_{2\hat{m}}^{(m)} + \overline{m}^2 F_{55}^{(m)} w_{3\hat{m}}^{(m)} + \left(\lambda_{z\hat{m}}^{(m-1)} - \lambda_{z\hat{m}}^{(m)}\right) = -\delta_{mn_l} q_{\hat{m}},\end{aligned} \tag{A22}$$

$$\begin{aligned}\delta w_1^{(m)}:\ &-\overline{m}A_{13}^{(m)}\,u_{0\hat{m}}^{(m)}+\left(-mB_{13}^{(m)}+mB_{55}^{(m)}\right)u_{1\hat{m}}^{(m)}+\left(-mD_{13}^{(m)}+2mD_{55}^{(m)}\right)u_{2\hat{m}}^{(m)}\\&+\left(-mF_{13}^{(m)}+3mF_{55}^{(m)}\right)u_{3\hat{m}}^{(m)}+\overline{m}^2B_{55}^{(m)}w_{0\hat{m}}^{(m)}+\left(A_{33}^{(m)}+\overline{m}^2D_{55}^{(m)}\right)w_{1\hat{m}}^{(m)}+\left(2B_{33}^{(m)}+\overline{m}^2F_{55}^{(m)}\right)w_{2\hat{m}}^{(m)}\\&+\left(3D_{33}^{(m)}+\overline{m}^2H_{55}^{(m)}\right)w_{3\hat{m}}^{(m)}+(-h_m/2)\left(\lambda_{x\hat{m}}^{(m-1)}+\lambda_{x\hat{m}}^{(m)}\right)=-\delta_{mn_l}\,(h_{n_l}/2)\,q_{\hat{m}}+N_{zt\hat{m}}^{(m)},\end{aligned}\tag{A23}$$

$$\begin{aligned}\delta w_2^{(m)}:\ &-2\overline{m}B_{13}^{(m)}\,u_{0\hat{m}}^{(m)}+\left(-2mD_{13}^{(m)}+mD_{55}^{(m)}\right)u_{1\hat{m}}^{(m)}+\left(-2mF_{13}^{(m)}+2mF_{55}^{(m)}\right)u_{2\hat{m}}^{(m)}\\&+\left(-2mH_{13}^{(m)}+3mH_{55}^{(m)}\right)u_{3\hat{m}}^{(m)}+\overline{m}^2D_{55}^{(m)}w_{0\hat{m}}^{(m)}+\left(2B_{33}^{(m)}+\overline{m}^2F_{55}^{(m)}\right)w_{1\hat{m}}^{(m)}+\left(4D_{33}^{(m)}+\overline{m}^2H_{55}^{(m)}\right)w_{2\hat{m}}^{(m)}\\&+\left(6F_{33}^{(m)}+\overline{m}^2J_{55}^{(m)}\right)w_{3\hat{m}}^{(m)}+\left(h_m^2/4\right)\left(\lambda_{z\hat{m}}^{(m-1)}-\lambda_{z\hat{m}}^{(m)}\right)=-\delta_{mn_l}\left(h_{n_l}^2/4\right)q_{\hat{m}}+2M_{zt\hat{m}}^{(m)},\end{aligned}\tag{A24}$$

$$\begin{aligned}\delta w_3^{(m)}:\ &-3\overline{m}D_{13}^{(m)}\,u_{0\hat{m}}^{(m)}+\left(-3mF_{13}^{(m)}+mF_{55}^{(m)}\right)u_{1\hat{m}}^{(m)}+\left(-3mH_{13}^{(m)}+2mH_{55}^{(m)}\right)u_{2\hat{m}}^{(m)}\\&+\left(-3mJ_{13}^{(m)}+3mJ_{55}^{(m)}\right)u_{3\hat{m}}^{(m)}+\overline{m}^2F_{55}^{(m)}w_{0\hat{m}}^{(m)}+\left(3D_{33}^{(m)}+\overline{m}^2H_{55}^{(m)}\right)w_{1\hat{m}}^{(m)}+\left(6F_{33}^{(m)}+\overline{m}^2J_{55}^{(m)}\right)w_{2\hat{m}}^{(m)}\\&+\left(9H_{33}^{(m)}+\overline{m}^2L_{55}^{(m)}\right)w_{3\hat{m}}^{(m)}+\left(-h_m^3/8\right)\left(\lambda_{z\hat{m}}^{(m-1)}+\lambda_{z\hat{m}}^{(m)}\right)=-\delta_{mn_l}\left(h_m^3/8\right)q_{\hat{m}}+3P_{zt\hat{m}}^{(m)},\end{aligned}\tag{A25}$$

$$\begin{aligned}\delta\lambda_x^{(k)}:\ &\left[u_{0\hat{m}}^{(k+1)}-(h_{k+1}/2)\,u_{1\hat{m}}^{(k+1)}+\left(h_{k+1}^2/4\right)u_{2\hat{m}}^{(k+1)}-\left(h_{k+1}^3/8\right)u_{3\hat{m}}^{(k+1)}\right]\\&-\left[u_{0\hat{m}}^{(k)}+(h_k/2)\,u_{1\hat{m}}^{(k)}+\left(h_k^2/4\right)u_{2\hat{m}}^{(k)}+\left(h_k^3/8\right)u_{3\hat{m}}^{(k)}\right]=0,\end{aligned}\tag{A26}$$

$$\begin{aligned}\delta\lambda_z^{(k)}:\ &\left[w_{0\hat{m}}^{(k+1)}-(h_{k+1}/2)\,w_{1\hat{m}}^{(k+1)}+\left(h_{k+1}^2/4\right)w_{2\hat{m}}^{(k+1)}-\left(h_{k+1}^3/8\right)w_{3\hat{m}}^{(k+1)}\right]\\&-\left[w_{0\hat{m}}^{(k)}+(h_k/2)\,w_{1\hat{m}}^{(k)}+\left(h_k^2/4\right)w_{2\hat{m}}^{(k)}+\left(h_k^3/8\right)w_{3\hat{m}}^{(k)}\right]=0,\end{aligned}\tag{A27}$$

where $m = 1, 2, \ldots, n_l$, and $k = 1, 2, \ldots, (n_l - 1)$.

Equations (A18)–(A27) represent a standard system of simultaneously linear algebraic equations. The displacement components and the transverse stress components induced in the FG beam can thus be determined by solving these equations. The secondary field variables, such as the in-plane stresses, can also be obtained using the constitutive equations.

References

1. Koizumi, M. FGM activities in Japan. *Compos. Part B* **1997**, *28*, 1–4. [CrossRef]
2. Koizumi, M. Recent progress of functionally graded materials in Japan. *Ceram. Eng. Sci. Proc.* **1992**, *13*, 333–347.
3. Shen, H.S. *Functionally Graded Materials: Nonlinear Analysis of Plates and Shells*; CRC Press: Boca Raton, FL, USA, 2009.
4. Reddy, J.N.; Chin, C.D. Thermomechanical analysis of functionally graded cylinders and plates. *J. Therm. Stresses* **1998**, *21*, 593–626. [CrossRef]
5. Miyamoto, Y.; Kaysser, W.A.; Rabin, B.H.; Kawasaki, A.; Ford, R.G. *Functionally Graded Materials: Design, Processing, and Applications*; Springer: New York, NY, USA, 1999.
6. Muller, E.; Drasar, C.; Schilz, J.; Kaysser, W.A. Functionally graded materials for sensor and energy applications. *Mater. Sci. Eng. A* **2003**, *362*, 17–39. [CrossRef]
7. Gerk, C.; Willert-Porada, M. Development of graded composite electrodes for the SOFC. *Mater. Sci. Forum.* **1999**, *308–311*, 806–813. [CrossRef]
8. Pompe, W.; Worch, H.; Epple, M.; Friess, W.; Gelinsky, M.; Greil, P.; Hempel, U.; Scharnweber, D.; Schulte, K. Functionally graded materials for biomedical applications. *Mater. Sci. Eng. A* **2003**, *362*, 40–60. [CrossRef]
9. Schulz, U.; Peters, M.; Bach, F.-W.; Tegeder, G. Graded coatings for thermal, wear and corrosion barriers. *Mater. Sci. Eng. A* **2003**, *362*, 61–80. [CrossRef]
10. Kumar, S.; Murthy Reddy, K.V.V.S.; Kumar, A.; Rohini Devi, G. Development and characterization of polymer-ceramic continuous fiber reinforced functionally graded composites for aerospace application. *Aero. Sci. Technol.* **2013**, *26*, 185–191. [CrossRef]
11. Sharma, N.K.; Bhandari, M. Review of sandwich beams with functionally graded core. *Int. J. Innov. Sci. Eng. Technol.* **2014**, *1*, 75–83.

12. Sayyad, A.S.; Ghugal, Y.M. Modeling and analysis of functionally graded sandwich beams: A review. *Mech. Adv. Mater. Struct.* **2019**, *26*, 1776–1795. [CrossRef]
13. Sankar, B.V. Thermal stresses in functionally graded beams. *AIAA J.* **2002**, *40*, 1228–1232. [CrossRef]
14. Trinh, L.C.; Vo, T.P.; Thai, H.T.; Nguyen, T.K. An analytical method for the vibration and buckling of functionally graded beams under mechanical and thermal loads. *Compos. Part B* **2016**, *100*, 152–163. [CrossRef]
15. Simsek, M. Fundamental frequency analysis of functionally graded beams by using different higher-order beam theories. *Nucl. Eng. Des.* **2010**, *240*, 697–705. [CrossRef]
16. Thai, H.T.; Vo, T.P. Bending and free vibration of functionally graded beams using various higher-order shear deformation beam theories. *Int. J. Mech. Sci.* **2012**, *62*, 57–66. [CrossRef]
17. Carrera, E. Theories and finite elements for multilayered plates and shells: A unified compact formulation with numerical assessment and benchmarking. *Arch. Comput. Methods Eng.* **2003**, *10*, 215–296. [CrossRef]
18. Giunta, G.; Crisafulli, D.; Belouettar, S.; Carrera, E. A thermo-mechanical analysis of functionally graded beams via hierarchical modelling. *Compos. Struct.* **2013**, *95*, 676–690. [CrossRef]
19. Carrera, E.; Filippi, M.; Zappino, E. Laminated beam analysis by polynomial, trigonometric, exponential and zig-zag theories. *Eur. J. Mech. A/Solids* **2013**, *41*, 58–69. [CrossRef]
20. Davalos, J.F.; Kim, Y.; Barbero, E.J. Analysis of laminated beams with a layer-wise constant shear theory. *Compos. Struct.* **1994**, *28*, 241–253. [CrossRef]
21. Mantari, J.L.; Oktem, A.S.; Soares, C.G. A new trigonometric layerwise shear deformation theory for the finite element analysis of laminated composite and sandwich plates. *Comput. Struct.* **2012**, *94–95*, 45–53. [CrossRef]
22. Wu, C.P.; Kuo, H.C. Interlaminar stresses analysis for laminated composite plates based on a local high order lamination theory. *Compos. Struct.* **1992**, *20*, 237–247. [CrossRef]
23. Wu, C.P.; Kuo, H.C. An interlaminar stress mixed finite element method for the analysis of thick laminated composite plates. *Compos. Struct.* **1993**, *24*, 29–42. [CrossRef]
24. Yang, Y.; Pagani, A.; Carrera, E. Exact solutions for free vibration analysis of laminated, box and sandwich beams by refined layer-wise theory. *Compos. Struct.* **2017**, *175*, 28–45.
25. Filippi, M.; Carrera, E. Bending and vibrations analyses of laminated beams by using a zig-zag-layer-wise theory. *Compos. Part B* **2016**, *98*, 269–280. [CrossRef]
26. Yazdani Sarvestani, H.; Akbarzadeh, A.H.; Mirabolghasemi, A. Structural analysis of size-dependent functionally graded doubly-curved panels with engineered microarchitectures. *Acta Mech.* **2018**, *229*, 2675–2701. [CrossRef]
27. Liew, K.M.; Pan, Z.Z.; Zhang, L.W. An overview of layerwise theories for composite laminates and structures: Development, numerical implementation and application. *Compos. Struct.* **2019**, *216*, 240–259. [CrossRef]
28. Vo, T.P.; Thai, H.T.; Nguyen, T.K.; Inam, F.; Lee, J. Static behavior of functionally graded sandwich beams using a quasi-3D theory. *Compos. Part B* **2015**, *68*, 59–74. [CrossRef]
29. Vo, T.P.; Thai, H.T.; Nguyen, T.K.; Inam, F.; Lee, J. A quasi-3D theory for vibration and buckling of functionally graded sandwich beams. *Compos. Struct.* **2015**, *119*, 1–12. [CrossRef]
30. Nguyen, T.K.; Vo, T.P.; Nguyen, B.D.; Lee, J. An analytical solution for buckling and vibration analysis of functionally graded sandwich beams using a quasi-3D shear deformation theory. *Compos. Struct.* **2016**, *156*, 238–252. [CrossRef]
31. Lü, C.F.; Chen, W.Q.; Xu, R.Q.; Lim, C.W. Semi-analytical elasticity solutions for bi-directional functionally graded beams. *Int. J. Solid Struct.* **2008**, *45*, 258–275. [CrossRef]
32. Reddy, J.N. *Mechanics of Laminated Composite Plates and Shells: Theory and Analysis*; CRC Press: Boca Raton, FL, USA, 2003.
33. Li, X.F.; Wang, B.L.; Han, J.C. A higher-order theory for static and dynamic analyses of functionally graded beams. *Arch. Appl. Mech.* **2010**, *80*, 1197–1212. [CrossRef]
34. Reddy, J.N. A simple higher-order theory for laminated composite plates. *J. Appl. Mech.* **1984**, *51*, 745–752. [CrossRef]
35. Touratier, M. An efficient standard plate theory. *Int. J. Eng. Sci.* **1991**, *29*, 901–916. [CrossRef]

36. Soldatos, K. A transverse shear deformation theory for homogeneous monoclinic plates. *Acta Mech.* **1992**, *94*, 195–220. [CrossRef]
37. Karama, M.; Afaq, K.S.; Mistou, S. Mechanical behavior of laminated composite beam by the new multi-layered laminated composite structure model with transverse shear continuity. *Int. J. Solids Struct.* **2003**, *40*, 1525–1546. [CrossRef]

Publisher's Note: MDPI stays neutral with regard to jurisdictional claims in published maps and institutional affiliations.

© 2020 by the authors. Licensee MDPI, Basel, Switzerland. This article is an open access article distributed under the terms and conditions of the Creative Commons Attribution (CC BY) license (http://creativecommons.org/licenses/by/4.0/).